Pioneering the industrialization of PERC technology: A review of the development of mono- and bifacial PERC solar cells at SolarWorld

Phedon Palinginis, Christian Kusterer, Stefan Steckemetz, René Köhler, René Härtwig, Torsten Weber, Matthias Müller, Gerd Fischer & Holger Neuhaus, formerly of SolarWorld Innovations GmbH / SolarWorld Industries GmbH

Abstract

SolarWorld has played a pioneering role in triggering and implementing the shift from p-type multicrystalline aluminium back-surface field (Al-BSF) to p-type monocrystalline passivated emitter and rear cell (PERC) as the next mainstream solar cell technology, and recognized PERC to be the door opener to an extremely simple and cost-effective implementation of a bifacial solar cell. This paper reviews PERC technology development at SolarWorld, featuring an *industrial* baseline process for monocrystalline five-busbar (5BB) p-type PERC solar cells exceeding 22.0% median (22.5% maximum) cell efficiency by May 2018, before operations at SolarWorld came to a final halt. One major distinguishing and very noteworthy aspect of the PERC technology employed at SolarWorld, which contrasts with mainstream PERC technology implementation, is the use of silicon oxynitride (SiO_xN_y) as rear-side passivation. Open-circuit voltages of 690mV are achieved, thus demonstrating the excellent passivation properties of the rear-side SiO_xN_y/SiN_z passivation stack. At this level, bulk carrier recombination needs to be addressed in an attempt to propel industrial p-type PERC towards > 24% cell efficiency *in mass production*. Therefore, extended attention is given to the results obtained from SolarWorld's dedicated effort to industrialize gallium-doped Czochralski (Cz-Ga) crystals in order to leverage potentially superior properties of Cz-Ga wafers, i.e. low bulk recombination and robustness against light-induced degradation at elevated temperatures. In a section dedicated to PERC bifacial, the paper addresses current weaknesses of PERC bifacial technology, and closes with an analysis of the limitations of 5BB p-type PERC bifacial solar cells as implemented at SolarWorld, namely 1) inevitable front-side efficiency losses compared with PERC monofacial, and 2) rear-side efficiency and thus bifaciality limitations imposed by the optical properties of the cell rear side.

Pioneering the industrialization of PERC technology under adverse market and business conditions

Still competing against different crystalline silicon solar cell architectures such as metal-wrap-through (MWT), emitter-wrap-through (EWT), interdigitated back-contact (IBC) and heterojunction (HJT) technology at the beginning of the 2010 decade, the passivated emitter and rear cell (PERC) concept has meanwhile established itself as the winning technology, which is currently in the midst of replacing Al-BSF solar cells as the mainstream product technology.

"PERC is currently in the midst of replacing Al-BSF solar cells as the mainstream product technology."

Facing increasing price pressures, SolarWorld pioneered the industrialization of PERC technology based on p-type monocrystalline substrates as early as 2012, with the twofold aim of differentiating technologically and occupying a niche market, ultimately trying to leverage a price premium for high-efficiency solar cells and modules. In doing so, SolarWorld helped substantially in carving out the industrial solar cell technology roadmap, pushing technology shares of the photovoltaic (PV) industry from p-type multicrystalline Al-BSF towards p-type monocrystalline PERC as the next mainstream solar cell technology, with significantly increased efficiency potential. In retrospect, the year 2012 proved to be pivotal on several levels (macro-economic, micro-economic, technological), as it marked:

- A distinct break within the growth phase of the global PV market, with annually installed global PV system capacity contracting for the first time in 2012 after over a decade of strong annual growth (Fig. 1(a)) [1–3].
- The tipping point for business operations at SolarWorld, with earnings before interest, tax, depreciation and amortization (EBITDA) slipping into the negative in 2012 as a result of the aforementioned global market contraction, oversupply and increasing price pressure (Fig. 1(b)).
- The technological tipping point marking 1) the industrialization of PERC technology, and 2) a correlated shift towards monocrystalline substrates, with SolarWorld ramping up its first p-type monocrystalline PERC line in 2012 as a dedicated first mover well ahead of the industry (Fig. 1(c) and (d)) [4–5].

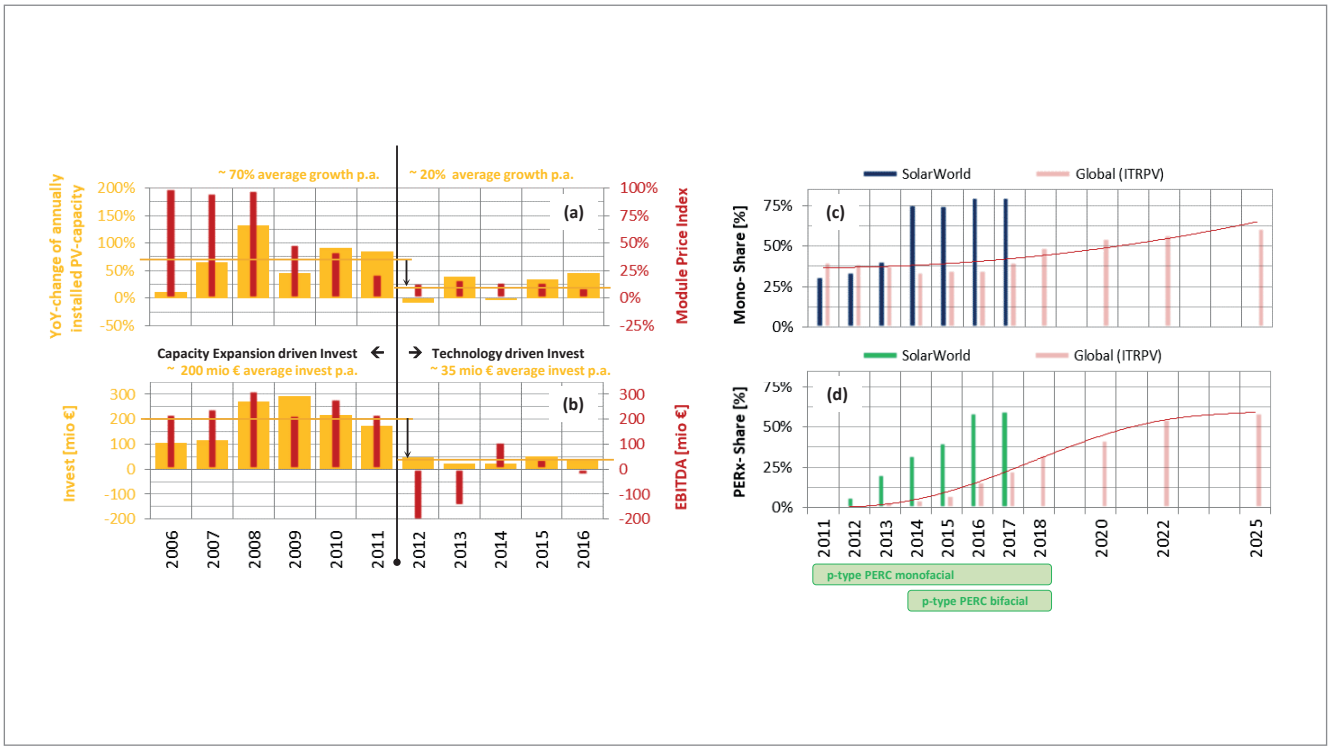

Figure 1. Pioneering the industrialization of PERC technology under adverse market and business conditions. (a) PV market growth: year-on-year (YoY) change of annually installed PV system capacity [1–2] and PV module price index as derived from BNEF [3] (Chinese c-Si modules [$/Wp, 2018 real], [ref. year: 2006]). (b) Evolution of annual investment volume and EBITDA at SolarWorld (annual reports). (c) Evolution of monocrystalline cell capacity share at SolarWorld vs. global evolution. (d) Evolution of p-type PERC capacity share at SolarWorld vs. global evolution of p/n-type PERx technology share. (Note: historical data of the global evolution in (c) and (d) are taken from the ITRPV roadmap editions of the respective years. Projected data for 2020 and onwards are taken from ITRPV 9th ed. (03/2018) [4].)

With EBITDA slipping into the negative, SolarWorld's investment budget (which up until then had mainly been allocated to production capacity expansions) dropped significantly by 2012, at a time when capital expenditures (CapEx) for technology-driven investments were needed to sustainably differentiate on a technological level. However, and despite persisting CapEx constraints as well as R&D quota just above 2%, PERC capacity was continuously ramped up at all three SolarWorld production sites in the 2012–2017 time frame, at a rate far exceeding that of the industry, as shown in Fig. 1(d). Increasingly adverse business conditions, however, put a halt to SolarWorld's PERC production capacity fraction at around 60% by the end of 2016. Further line conversions planned for 2017 and the following years had to be cancelled. With monocrystalline wafers levering the technological advantages of PERC to the fullest, the shift towards PERC technology within SolarWorld was also accompanied by a dedicated technological-strategic shift towards *monocrystalline* solar cells. This measure was supported by the acquisition of Bosch Solar Energy as a pure play, p-type monocrystalline Al-BSF cell manufacturer at the end of 2013. By 2016, all SolarWorld PERC lines were operating with monocrystalline wafers, whereas the final remaining production capacity share of multicrystalline cell lines operating with Al-BSF had dropped to below 20%.

In summary, SolarWorld not only helped to introduce PERC technology to the PV market, but also anticipated the shift towards monocrystalline technology well ahead of the industry, with PERC and diamond-wire (DW) wafering setting up the game-changing triggers. Furthermore, SolarWorld developed and launched a highly cost-effective PERC bifacial solar cell variant which has led to unprecedented hype regarding bifacial technology. In the end, SolarWorld was not able to implement a full conversion to PERC, given the increasingly adverse business conditions leading to company insolvency. Credit is due to the former SolarWorld R&D and engineering staff responsible for the pioneering work on industrializing PERC technology at SolarWorld, as well as to the universities, R&D institutes and key equipment and material manufacturers for their instrumental contributions along this path.

PERC technology implementation at SolarWorld

Today, the dominant implementation of PERC technology with over 90% technology share is based on plasma-enhanced chemical vapour deposition (PECVD) of aluminium oxide (AlO_x)/silicon nitride (SiN_z) stacks for rear-side passivation and increased rear reflection (light trapping) [4,6,7]. Even though SolarWorld did ramp up PERC AlO_x using *remote* plasma technology on one of its production lines, and developed

PERC AlO_x using *direct* plasma technology on its R&D pilot line, the initial industrialization of PERC technology at SolarWorld, as well as the successive conversion of Al-BSF to PERC lines, was based on PECVD deposition of SiO_xN_y/SiN_z rear-side stacks [8]. Independently of the passivation stack employed, local contact opening (LCO) of the rear-side dielectric via laser ablation is used [9,10] to enable rear-side contacting and local Al-BSF formation employing full-area Al screen printing and making use of local Al-Si alloying during fast firing [11]. Before opting for LCO and Al screen printing as the preferred technology for implementing local rear contacts, SolarWorld had been working up until 2011 on an industrial PERC implementation based on thick thermal oxide as the rear-side passivation layer, Al evaporation or Al screen printing for metallization, and laser-fired contacts (LFC) for rear-side contact formation [12]. The approach was abandoned mainly for technological reasons, i.e. excessive contact recombination inherent in the LFC approach limiting cell efficiency [13].

Fig. 2 reiterates the generic advantages of PERC technology. The distinctive features, representing the best-known methods (BKM) of SolarWorld's industrial PERC baseline process as of 05/2018, are highlighted below:

- Base material: Ga-Czochralski (Cz) wafers.
- Process flow: rear-side polishing and passivation before front-side texturing and diffusion [8].
- Single processes:
  - o Rear-side passivation: SiO_xN_y/SiN_z using direct PECVD (adapted stack for bifacial).
  - o Emitter: selective emitter (SE) using laser doping from phosphorus silicate glass (PSG).
  - o Emitter passivation: thermal oxidation using tube furnaces.
  - o 5BB metallization rear: floating silver (Ag) pads. Aluminium grid (for bifacial).
  - o 5BB metallization front: single print, *actively* aligned on SE.

For completeness, the well-known benefits of the SE and rear-side passivation with respect to increasing solar cell performance are shown in Fig. 2(c): the SE leads to an improved blue response when compared with a homogeneous emitter, while the rear-side passivation shows an improved infrared (IR) response when compared with an Al-BSF solar cell as a result of improved passivation and light trapping. The improved spectral response (internal quantum efficiency in Fig. 2(c)) gives rise to a short-circuit current gain, whereas improved emitter and rear-side passivation both contribute to a gain in open-circuit voltage as shown in Fig. 2(b).

The following sections highlight the main technological measures which have allowed an increase in *median* solar cell efficiency of *industrial* monocrystalline PERC SiO_xN_y solar cells from 20.0% to 22.0% in the 01/2015–05/2018 time frame on the R&D PERC cell pilot line in Freiberg, Germany.

PERC SiO_xN_y/SiN_z monofacial: evolution of the industrial PERC baseline process on the R&D pilot line

This section provides a review of the main PERC solar cell R&D activities at SolarWorld carried out within the 01/2015–05/2018 time frame, enabling the performance improvements shown in Fig. 3 of the industrial PERC SiO_xN_y/SiN_z baseline process on the R&D cell pilot line at SolarWorld.

Emitter/emitter passivation

At the beginning of 2015, the overall share of solar cell line capacity at SolarWorld running SE technology already stood at almost 70%, far exceeding the corresponding global share of ~5% for SE technology at that time (ITRPV 7th edn). The homogeneous emitter (HE) technology on the remaining cell production lines was based on a $POCl_3$ process which had been successfully developed by the University of Konstanz. Aimed at reducing emitter saturation currents at sheet resistances of the order of 80–100Ω/sq., the underlying approach was chosen to reduce the amount of phosphorus precipitates, and thus the amount of inactive phosphorus present in the emitter, mainly by adjusting the $POCl_3$-N_2 gas flow during the deposition phase [14]. The thus-formed HE places stringent requirements not only on the $POCl_3$-diffusion process itself, but also on the front-side silver (Ag) paste selection as well as the firing conditions to ensure acceptable contact formation. Before being transferred to SolarWorld, the $POCl_3$ process was optimized using a design-of-experiment (DoE)-based approach. Final open-circuit-voltage levels reached 660mV on the R&D pilot line at the beginning of 2015 using direct plasma deposited SiN_x as the emitter passivation and anti-reflection coating (ARC). Up until then, the R&D PERC monofacial baseline process served to ensure a stable operation of this emitter type on the remaining HE cell lines in production.

With simulation-guided optimization [15] still identifying the HE as the largest recombination channel, further measures for emitter optimization were implemented in 2015 on the R&D pilot line. First, the PERC baseline was switched to SE technology [16], already available on the R&D pilot line. Second, dry thermal oxidation for improved emitter passivation, which had been investigated at SolarWorld starting in 2012 [17], was introduced with support from the process engineers of the Arnstadt site (former Bosch Solar Energy). Reduced emitter saturation currents well below 50fA/cm² were thus achieved via improved surface passivation, phosphorus activation and phosphorus drive-in

– all simultaneously occurring during the tube furnace process [17,18]. The successive introduction of SE and thermal oxidation can be identified as step-like improvements in open-circuit voltage. Both measures were part of a device optimization strategy primarily guided by the suppression of recombination channels, thus increasing open-circuit voltage.

Base passivation

Representing the passivation technology of choice for PERC implementation at SolarWorld, the R&D pilot line baseline data shown in Fig. 3 exclusively reflect the performance of the monofacial PERC process using SiO_xN_y/SiN_z rear-side stacks and direct PECVD tube furnaces for deposition of the dielectric layers [8]. One important activity, which had already started in Q2 2014, was the design and the corresponding process development of a SiO_xN_y/SiN_z rear-side stack adapted and optimized for bifacial operation (not shown). In parallel, a PERC AlO_x process based on direct PECVD tube furnaces was also developed, investigating whether a thus-deposited stack does indeed show superior performance over SiO_xN_y/SiN_z [19,20]. Furthermore, a PERC AlO_x process sequence based on remote PECVD [7] as the current mainstream technology was developed and ramped up on one production line.

Regardless of the PERC AlO_x/SiN_z process used, the main challenge from a process integration point of view – which was successfully resolved – was to integrate emitter passivation via thermal oxidation in a PERC AlO_x process flow. Ultimately, with the SiO_xN_y/SiN_z stack exhibiting effective surface recombination velocities (S_eff) as low as 15cm/s [18], SolarWorld kept with PERC SiO_xN_y as the (passivation) technology of choice for further line conversions throughout its PERC ramp-up activities.

Figure 2. Transitioning from Al-BSF to PERC at SolarWorld.
(a) Design and process changes:
- **Rear side: Rear-side passivation: SiO_xN_y/SiN_x using PECVD direct plasma.**
- **Rear side: Local contact opening (LCO): laser ablation @ 532 or 1064nm.**
- **Front side: Selective emitter (SE): laser doping from PSG @ 532nm.**
- **Front side: Emitter passivation: dry thermal oxidation using tube furnace.**

(b) Comparison of current–voltage characteristics.
(c) Comparison of internal quantum efficiency: enhanced internal photon conversion in the UV as a result of SE, and in the IR as a result of rear-side passivation.

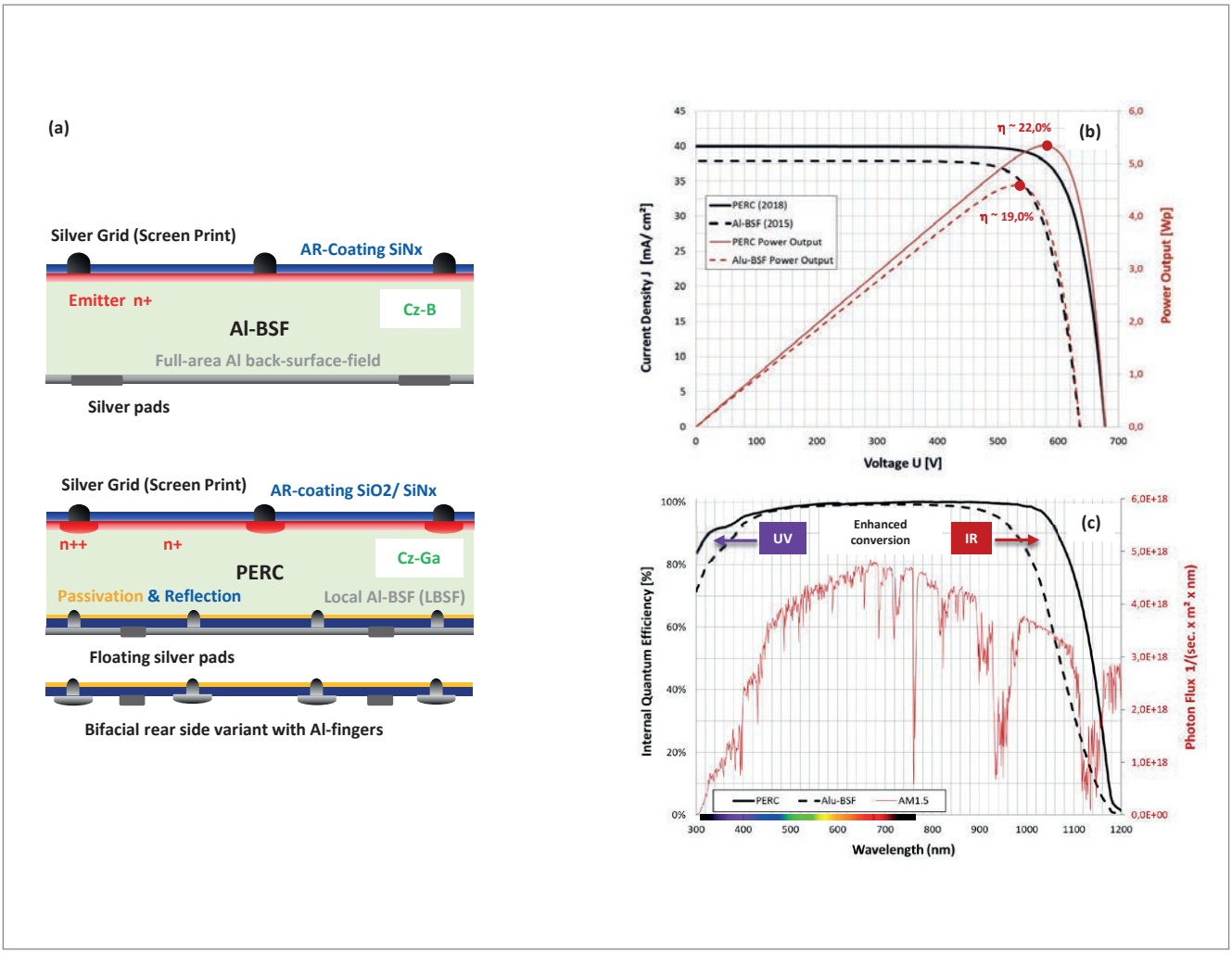

Contacting and metallization

Within the dedicated recombination-suppressing device optimization strategy, contact features were consequently and continuously miniaturized:

- Front side: reduction of the selective emitter regions to 130µm finger width. Continuous reduction of screen-printed Ag fingers, reaching 30µm finger width with state-of-the art meshes and Ag pastes.
- Rear side: switch from a line to a dashed layout, reaching LCO area fractions well below 2%.

With the early introduction of 5BB technology at SolarWorld starting in 2015 and the outlook towards zero-busbar technology (0BB), SolarWorld's extensive efforts to develop an extrusion printing technology for high-aspect-ratio fine-line printing were finally abandoned at the beginning of 2015 [21] in order to fully focus on single screen printing as the technology of choice. Anticipating the necessity for active alignment at ever-decreasing contact feature sizes, SolarWorld installed a novel screen printer on the R&D pilot line in 2016, featuring in situ recognition of the patterns to be metallized, allowing:

- Active positioning of front-side Ag screens on SE-patterns.
- Active positioning of rear-side Al screens on LCO patterns for PERC bifacial.

Metallization layouts for 0BB technology were developed and tested on Solarworld's proprietary multiwire stringer built by USK Karl Utz Sondermaschinen GmbH. The machine combined a laser to produce *half-cut cells,* a wire field, contact soldering and laser separation of the wires to form the entire 120-half-cell matrix in a continuous process with a throughput of 3,600 full cells per hour [22]. In addition, multiwire modules with *full cells* were built with the help of Meyer Burger Germany GmbH using their SmartWire Connection Technology (SWCT), reaching 320Wp for a 60-cell glass–backsheet module employing an industrial module bill of materials (BOM) only.

Base recombination

As part of PERC development, bulk properties were studied intensively at theoretical [23] and experimental levels at SolarWorld, with recognition that for the efficiency potential of PERC to unfold, low *and* stable material recombination currents ($j_{0,mat}$) are required. Consequently, several highly innovative crystallization technologies were developed at SolarWorld by the crystal R&D team as well as by production engineers. Both approaches followed the strategy of reducing interstitial oxygen [Oi] in the crystal analogously to magnetic Czochralski (MCz) and float zone (FZ), yet keeping it economically viable:

"With the SiO_xN_y/SiNz stack exhibiting effective surface recombination velocities (S_eff) as low as 15cm/s, SolarWorld kept with PERC SiO_xN_y as the (passivation) technology of choice."

- Cast monosilicon (or quasimono): with the use of appropriately oriented Cz crystal slabs as well as full-area seeds, a proprietary variant of quasimono technology was extensively developed and transferred to production. Already by the end of 2014, a world-record p-type cast monosilicon PERC solar cell from the R&D pilot line exhibiting >21.4% cell efficiency [21] demonstrated the excellent bulk crystal quality of SolarWorld's cast monosilicon material. Bulk lifetimes for cast monosilicon wafers exceeding those in Cz-grown silicon were demonstrated [24] thanks to the low interstitial oxygen content $[O_i] \sim 1–2\times10^{17}$at/cm^3 inherent in crystal casting technology and to a deep understanding of dislocation density control during seeding [25].

- NeoGrowth: another proprietary crystal growth technique, termed *NeoGrowth*, which uses a contactless bulk crystal growth method for producing single crystal ingots, was developed at SolarWorld, aimed at providing monocrystalline wafers at lower cost than Cz-grown wafers [26]. This being a contactless technology, the oxygen content can be kept to below $[O_i] \sim 1–2\times10^{17}$at/cm^3. With liquid silicon being continuously fed onto a crystalline silicon seed layer, the otherwise segregation-driven resistivity span over the crystal height can be significantly reduced, allowing low resistivity wafers (~1.0Ωcm) to be tailored at a tight resistivity distribution in favour of PERC solar cells, which require low base/spreading resistance.

Not having reached technological maturity and chasing after 'moving' cost targets, the development of both crystal technologies was overtaken by the rapid price decline of Cz-grown wafers as the incumbent technology. With the demonstration of world-record PERC efficiencies of 21.7% (07/2015) and 22.0% (12/2015) on the R&D PERC pilot line at SolarWorld using Ga-doped Cz-grown monocrystalline wafers [27,28], the decision was thus made in 2016 to pilot Ga-doped Cz crystals at SolarWorld to further increase the efficiency of PERC solar cells, despite the lack of in-house continuous Cz (CCz) technology for achieving tight resistivity control.

While the R&D pilot line served to sample and assess the quality of the above-mentioned crystals as well as other substrate types, the baseline as shown in Fig. 3 strictly reflects the performance

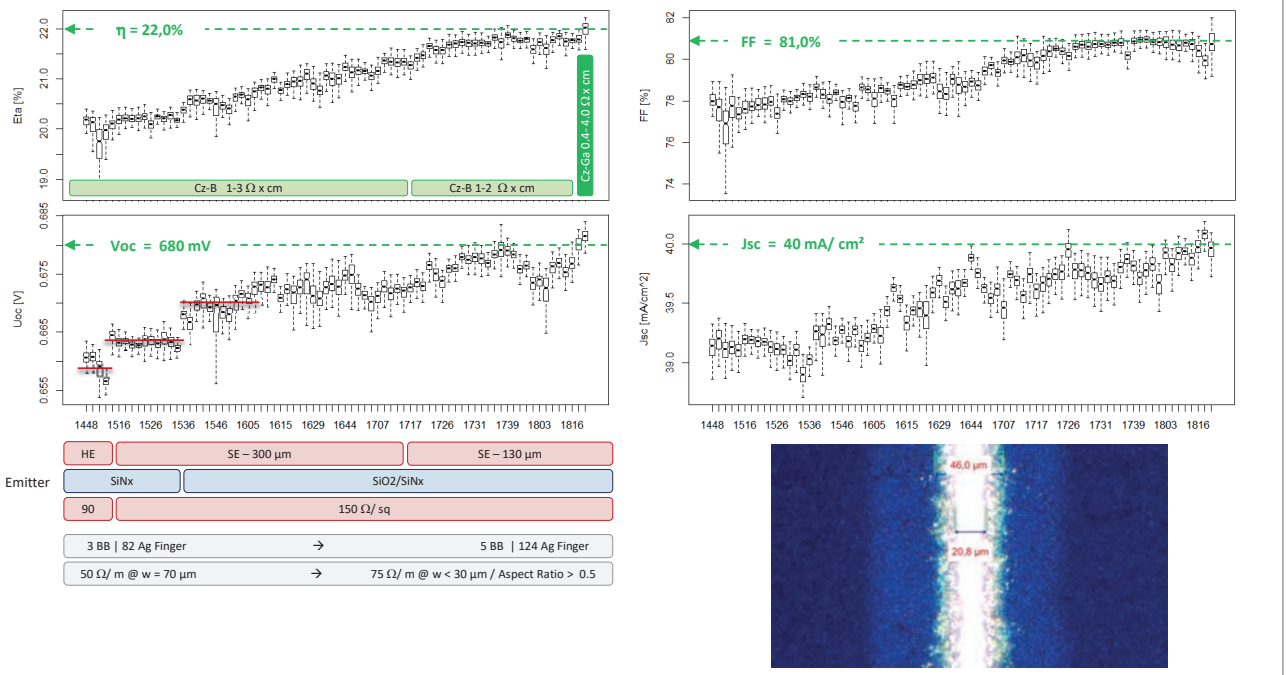

Figure 3. Evolution of the industrial PERC monofacial baseline process on the R&D PERC cell line at SolarWorld. The *I–V* measurement is calibrated against CalLab-certified reference cells, which were continuously updated upon significant design/process changes. The baseline ID is indexed as YYww. The best-known method 05/2018 exceeds 22.0% median cell efficiency and 680mV open-circuit voltage. The open-circuit voltage reveals stepwise improvements in emitter (passivation) technology. The early transition from 3BB to 5BB allowed the limits of screen printing to be continuously pushed towards finger widths (as printed) <30µm. The introduction of a novel SE laser process with a focal width of 130µm, in combination with a novel front-side printer using in situ pattern recognition for active print alignment in 2016, allowed further and continuous reduction of contact-related V_{oc} losses. The inset bottom right shows an optical microscope image of a front-side Ag-finger. The n^{++} region of the SE underneath can also be seen in the contrast. The Ag finger is well centred as a result of active alignment.

based on commercially available Cz-B wafers (internally or externally sourced), with the only measure being the tightening of the resistivity specification. The final baseline run was carried out using Cz-Ga material from an in-house Cz pull, to achieve a median cell efficiency exceeding 22.0% for an industrially relevant process. The best cell from a sister run yielded an ISE-CalLab-certified open-circuit voltage of V_{oc} = 688.5mV and a cell efficiency of η = 22.5% for a fully industrial 5BB Cz-Ga PERC cell, demonstrating the excellent recombination properties of Cz-Ga bulk as well as SiO_xN_y/SiN_z rear-side passivation.

Base material choice – Cz-Ga vs. Cz-B

Sticking with p-type technology, the alternative strategy for achieving high initial, and above all stable, bulk lifetime – other than reducing $[O_i]$ content in the crystal – is the switch from boron to gallium as the p-type dopant [29–31]. The main technological barrier of entry for the industrialization of Cz-Ga crystals and wafers for crystalline silicon solar cells is the low segregation coefficient of Ga (k = 0.008), which results in a wide resistivity span over the ingot height. Crystallization technologies based on a continuous feeding of silicon (such as CCz or NeoGrowth), however, can overcome this issue and produce essentially flat resistivity profiles over the ingot height [32].

In the following, the results of a dedicated material study benchmarking Cz-Ga against Cz-B crystals/wafers are summarized. Practically relevant benchmark metrics contained in the extended *I–V* dataset of Cz-B/Cz-Ga PERC solar cells at efficiency levels/V_{oc} levels of 22.0%/680mV respectively are applied. Initial, degraded and regenerated bulk lifetimes for Cz-B/Cz-Ga base materials in *post-cell-process* conditions are also presented, underlining the corresponding *I–V* parameter evolution for Cz-B/Cz-Ga PERC solar cells exposed to illumination at elevated temperatures. Since in-house CCz-puller capability was lacking, the crystals were grown in-house using semi-continuous (or recharge) RCz technology available at SolarWorld. It is shown that, despite the segregation-inherent resistivity span, RCz grown Cz-Ga wafers can offer a superior substrate choice over RCz-grown Cz-B wafers, despite the strong segregation of gallium.

Additional equipment for cell regeneration is not needed, given the robustness of Cz-Ga base material against illumination at elevated temperatures.

Cz-Ga vs. Cz-B – Part 1: Initial (as-flashed) *I–V* data

In Fig. 4 the as-flashed *I–V* data of an experimental cell run that was simultaneously carried out on two Cz-B wafer reference batches and one Cz-Ga wafer batch are shown. The Cz-B wafer batches were randomly chosen from the deliveries of two external Tier 1 wafer suppliers (S-1, S-2), both exhibiting base resistivities in the range 1.0–2.0Ωcm. The Cz-Ga wafer batch originated from an in-house Cz crystal run (2016) and was split into four sub-batches, with wafers from each sub-batch originating from four ingot sections (Sec 1 = tail, Sec 2 = tail-centre, Sec 3 = top-centre, Sec 4 = top) making up the full crystal (where *top* denotes the seed end). The segregation-inherent resistivity range for the Ga-doping level chosen corresponds to 0.4–4.0Ωcm. All wafers have M2 format and are diamond-wire cut. To ensure consistent cell-processing conditions, all wafer batches were homogenized into one single batch prior to processing. The cell process employed reflects the baseline BKM 05/2018 of the final run shown in Fig. 3. The *I–V* data for the Cz-Ga sub-batches are shown separately for each ingot section to illustrate the dependence on crystal height. The data of all four sections are consolidated in the box termed *Cz-Ga-all* to benchmark the overall performance of the complete, ingot-representative, Cz-Ga wafer ensemble with the Cz-B reference batches.

The as-flashed and hysteresis-free *I–V* measurement reveals superior performance of the Cz-Ga PERC cell batch, with a median cell efficiency exceeding that of the still undegraded Cz-B PERC reference batches by $\Delta\eta > 0.10\%_{abs}$. The broad base-resistivity range manifests itself within the broad lumped cell series resistance (*S*_ser), and correspondingly the fill factor (*FF*) distribution. *S*_ser (*FF*) increases (decreases) from tail (Sec 1) to top (Sec 4) in line with expectation. It is mainly the spread in *FF* that determines the broader efficiency distribution of the Cz-Ga batch. Whereas V_{oc} is constant over the crystal height for the PERC cell design chosen, the short-circuit current density starts to drop in the tail region of the Cz-Ga crystal, indicating decreased carrier lifetimes for resistivities below 0.5Ωcm. The *S*_ser data confirm a similar base resistivity (1.0–2.0Ωcm) of the Cz-B reference batches and Sec 2 of the Cz-Ga batch, as expected, from the resistivity profile of the Cz-Ga ingot. Most interestingly, a higher pseudoFF (*pFF*) can still be observed for the Cz-Ga PERC cells, implying higher bulk carrier lifetimes at similar doping levels as well as a generally superior injection dependence of the carrier lifetime for Cz-Ga base material in the initial state. Superior bulk properties are also reflected within a V_{oc} gain of the order of 3mV, and correspondingly lower saturation currents J_{01} of the Cz-Ga PERC cells, with J_{01} decreasing from tail (100fA/cm²) to top (85fA/cm²).

In the next two sections, the degradation/regeneration behaviour of the different wafer types is presented.

Cz-Ga vs. Cz-B – Part 2: Evolution of *I–V* data under illumination at elevated temperatures

For each of the six wafer batches (two Cz-B reference batches and four Cz-Ga sub-batches), ten cells were randomly picked and subjected to illumination at elevated temperatures (0.5 Suns/75°C) for 180h. The evolution of the *I–V* parameters, after normalization to their initial state prior to degradation, is shown in Fig 5. Since the evolution of the normalized *pFF* matches that of the normalized *FF* for all samples, *pFF* is not shown separately. Note that no major differences in the degradation behaviour of Cz-Ga PERC cells originating from different crystal sections are observed; the data of all Ga batches (Sec 1–4) are therefore consolidated in the graphs. Distinctively different behaviours within the time frame of the measurement are observed for:

- **Cz-B | S-1.** This sample shows a degradation and regeneration behaviour which is typical of BO-related light-induced degradation (LID). At the lowest power point (LPP), a substantial relative efficiency loss of the order of 6% is monitored. All *I–V* parameters shown regenerate to their initial values to within 1%, within the time frame of the measurement.

- **Cz-B | S-2.** This sample not only shows a more severe degradation, with over 8% relative efficiency loss at LPP, but also a more persistent degradation, with only some initial signs of regeneration within the time frame of the measurement. This behaviour, which is characteristic of light and elevated-temperature induced degradation (LeTID) observed in multicrystalline PERC cells, has been reported by Hanwha Q CELLS to also occur in p-type Cz PERC cells [33] and is herein confirmed.

  Note that, for both Cz-B PERC reference batches investigated, the magnitude of the observed degradation is of similar order for the *I–V* parameters *FF* / V_{oc} / J_{sc}, with only a slight trend in decreasing contribution from *FF* (highest relative degradation) → V_{oc} → J_{sc} (lowest relative degradation) to the overall relative efficiency degradation.

- **Cz-Ga all.** In contrast to both Cz-B PERC cell batches, Cz-Ga PERC solar cells exhibit a significantly lower relative efficiency loss

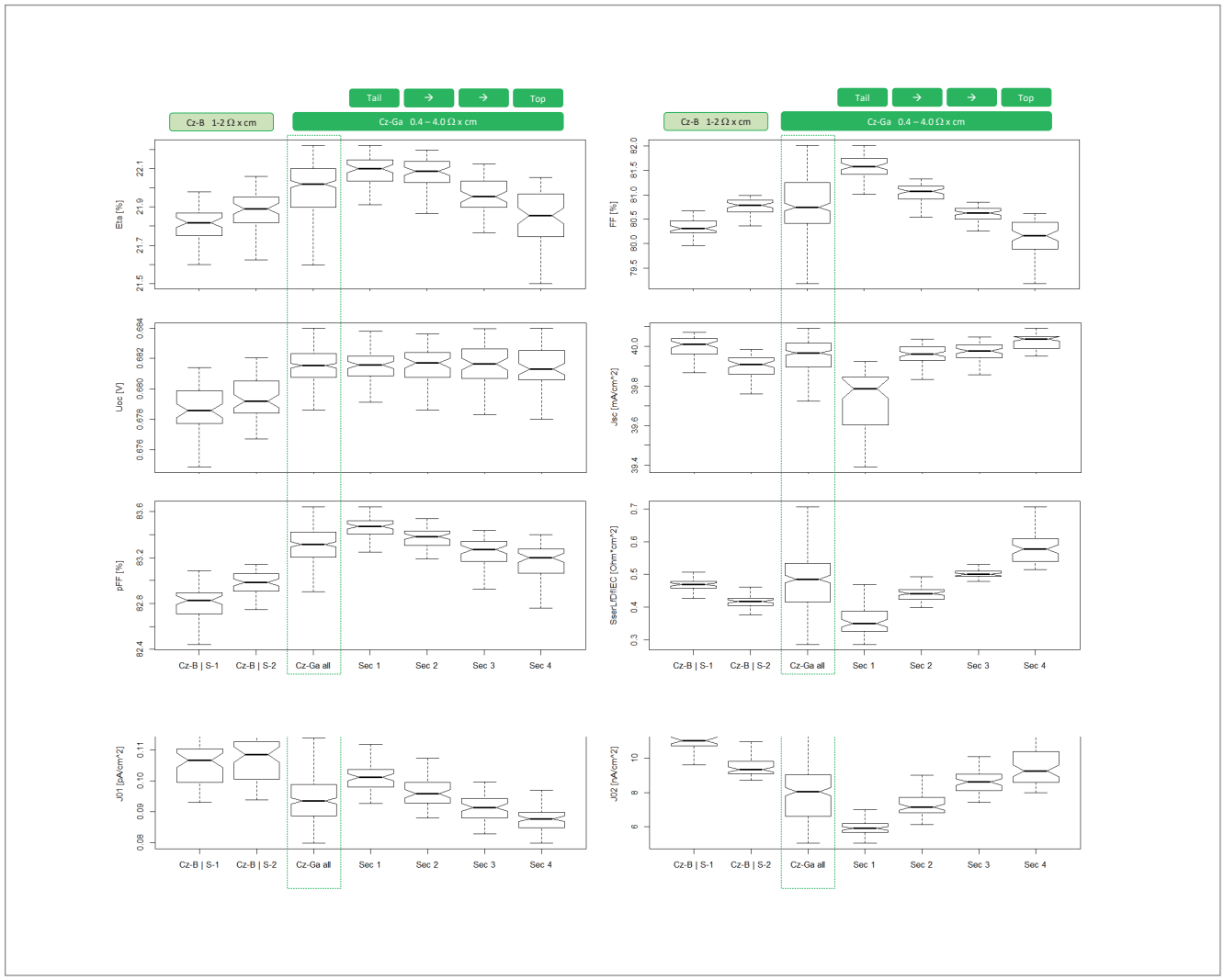

Figure 4. As-flashed, hysteresis-free *I–V* data for Cz-B and Cz-Ga PERC Cells. Two Cz-B reference batches (S-1 and S-2) are included. To illustrate the effect of the large resistivity span for Cz-Ga, the Cz-Ga batch is split into four sub-batches, corresponding to the four ingot sections (Sec 1: tail, Sec 4: top).

of the order of 1.5% within the time frame of the measurement, irrespective of longitudinal position within the crystal. As opposed to the Cz-B reference batches, J_{sc} and V_{oc} show almost no signs of deterioration. In particular, the slight efficiency loss observed is solely driven by a slight loss in *pFF*. As in the case of batch Cz-B | S-2, a persistent component can be observed in the *pFF*, reflecting a deterioration of the injection dependence of the bulk carrier lifetime, which is strongly suppressed, however, for Ga-doped Cz PERC cells. Within the two-diode fitting procedure underlying the *I–V* dataset, a persistent degradation also appears in the saturation current of the second diode (J_{02}). Reflecting changes in (the injection dependence of) bulk carrier lifetime, *pFF* and J_{02} should be closely monitored when signatures of LeTID are observed in the *I–V* parameters of, for example, Cz-B- or Cz-Ga-based PERC solar cells.

"No major differences in the degradation behaviour of Cz-Ga PERC cells originating from different crystal sections are observed."

To summarize, superior bulk performance of Cz-Ga wafers over Cz-B wafers is observed on the basis of the *I–V* parameters in the initial state and after illumination at elevated temperatures for high-efficiency industrial PERC solar cells at an efficiency level of 22.0%. Consistency of this result with the evolution of initial, degraded and regenerated bulk lifetime data of *post-process* Cz-B and Cz-Ga base materials is presented in the next section.

Cz-Ga vs. Cz-B – Part 3: Evolution of bulk carrier lifetime: initial – degraded – regenerated state

In order to obtain a better understanding of carrier lifetime-limiting defects for Cz-B and Cz-Ga base materials in fully processed PERC solar cells, and in order to correlate experimentally determined bulk carrier lifetimes in a *post-process condition* with corresponding *I–V* parameters, lifetime measurements have been carried out on different materials subjected to two different cell processing conditions (R&D pilot line vs. production line).

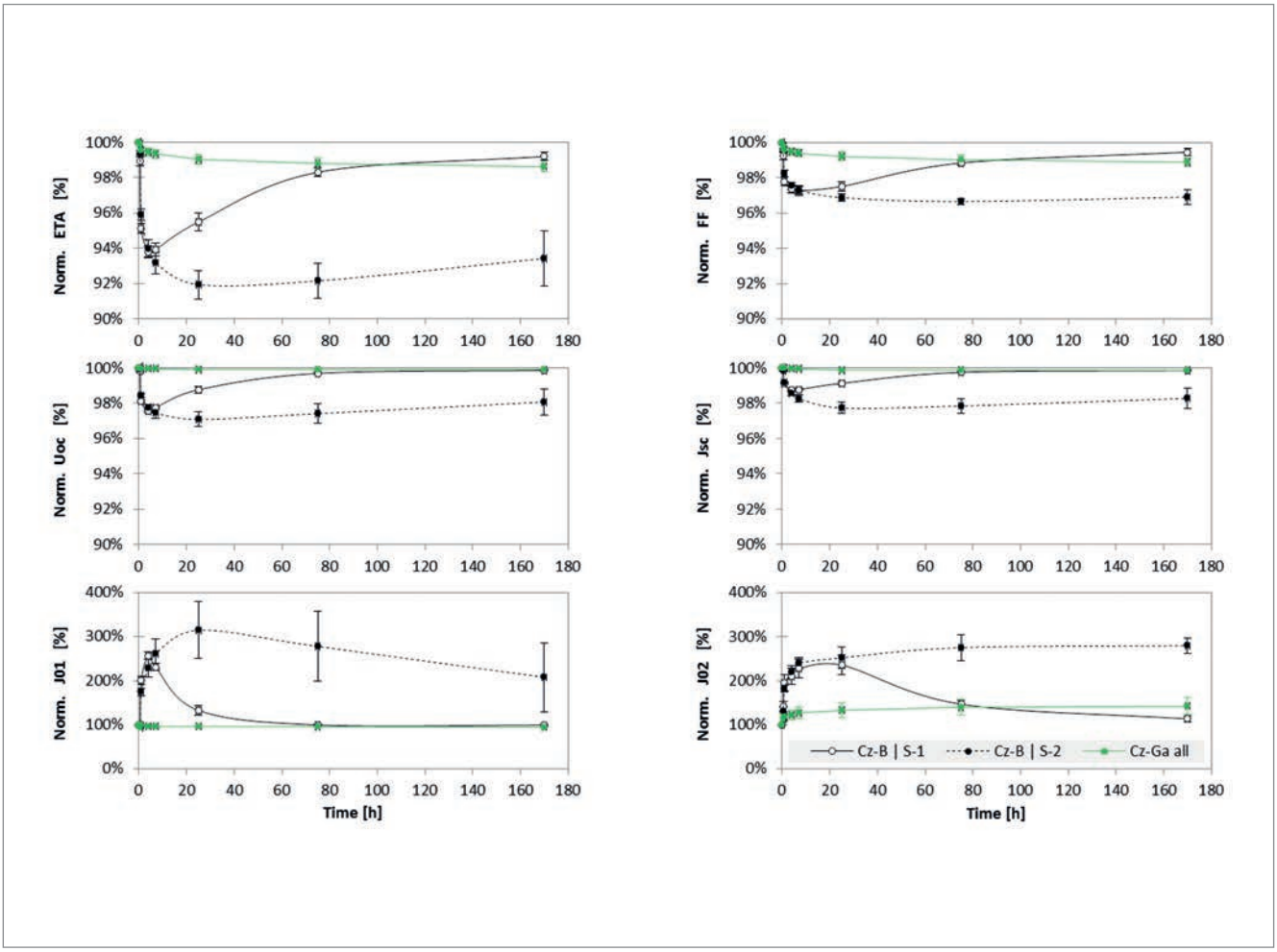

Figure 5. Degradation under illumination at elevated temperatures (0.5 Suns @ 75°C). For Cz-Ga, all ingot sections 1–4 are consolidated in one graph (40 cells total). Batch Cz-B | S-1 exhibits typical BO-driven LID behaviour, while Cz-B | S-2 exhibits an additional LeTID component. In contrast to the Cz-B reference batches, degradation is strongly suppressed in the Cz-Ga PERC cell batch.

Fig. 6 shows photoconductance decay (PCD) lifetime measurements recorded with a WCT-120 Sinton tool for Cz-B and Cz-Ga base materials. Rather than testing 'typical' lifetime samples, as (for example) prepared in Walter et al. [34], it was chosen to investigate the bulk carrier lifetime in wafers which have undergone full PERC processing in order to include within the measured bulk carrier lifetimes the impact of 1) the thermal budget/history of the particular cell process, and 2) potential contamination sources of the particular cell process affecting the base material. Metallization and dielectric layers were thus chemically removed from fully processed PERC solar cells by the analytic laboratory at SolarWorld in order to recover the bare bulk wafer and to determine *post-cell-process bulk carrier lifetimes at injection levels corresponding to the maximum power point (mpp)* [23]. In a similar way to the procedure described in Walter et al. [34], the recovered bare wafers were both-side passivated (ALD-AlO_x/PECVD-SiN_x) and fired (note that the substrates were *not* diffused, since they had already undergone diffusion during cell processing). PCD measurements were carried out 1) in the initial state, 2) after degradation (0.1 Sun @ 30°C for 72h), and 3) after regeneration (1.0 Sun @ 185°C for 15 min.). Lifetime sample passivation, firing, conditioning and PCD measurements were performed at the Institute for Solar Energy Research in Hamelin (ISFH).

Independently of the crystal growth process ('Crystal 1/2') and the cell process employed ('R&D Pilot Line'/'Production Line'), the Cz-Ga substrates show similar bulk carrier lifetimes. Note that, given the excellent passivation quality of the ALD-AlO_x/PECVD-SiN_z passivation with recombination velocities <1cm/s [34], the carrier lifetimes measured correspond to bulk defect recombination. Bulk carrier lifetimes in Cz-Ga base materials do not change when subjected to typical degradation and regeneration procedures. In contrast, the Cz-B lifetime samples (the original cells of which had been simultaneously processed with sample 'Cz-Ga Crystal 2 – Production Line'), show severe bulk carrier lifetime degradation, which can, however, be recovered within a regeneration process. On the basis of these carrier lifetime data, the impact of interstitial iron Fe_i as a potential bulk carrier lifetime-limiting defect in Cz-Ga is discussed, following a simple Shockley-Read-Hall (SRH) analysis.

Cz-Ga vs. Cz-B – Part 4: FeGa vs. FeB defects – SRH analysis

With iron being one of the most critical contaminants in crystalline silicon [35], the question arises whether the experimentally determined bulk carrier lifetimes in Fig. 6 are in line with –and potentially limited by – an Fe-related defect in the Ga/B-doped Cz-crystals. It is well known that electrically active iron-acceptor (FeX) pairs are formed in p-type crystalline silicon as a result of Coulomb attraction between highly mobile, positively charged interstitial iron Fe_i and negatively charged substitutional acceptors (X = B, Al, Ga, In) [36,37]. The characteristic of such FeX defects is that they can be dissociated via light stimulation within minutes [38]. Re-association kinetics are found to be independent of the dopant species (X). Timescales for re-association in the dark are higher than dissociation timescales and vary, depending on dopant concentration [X], from several minutes (ρ_{base} ~ 0.5Ωcm) to over one hour (ρ_{base} ~ 4.0Ωcm) [39]. With the Fe_i defect showing a strong injection dependence in the fully dissociated state, and the associated FeX

"Despite careful sample conditioning, the degree of iron-acceptor association/dissociation is difficult to determine experimentally."

defects showing a weak injection dependence, a dopant-characteristic crossover point of the SRH lifetimes is observed. This feature is at the base of a highly sensitive iron detection method, which was first developed for boron-doped silicon [38] and later extended to Ga-doped silicon [40]. In Schmidt & Macdonald [40], SRH parameters have been determined for the dominating FeGa defect in intentionally Fe-contaminated Cz-Ga samples, assuming that the lifetime in the associated state is solely determined by the deeper level FeGa defect which corresponds to the trigonal configuration of the FeGa pair [37,40].

Fig. 7 shows the analytical results for the SRH lifetime and the material saturation current density $j_{0,mat}$ as a function of base resistivity and at carrier injection levels corresponding to mpp conditions [23]. The iron level is set to $[Fe_i]$ = 1.5×10^{10}at/cm^3. The SRH parameters for Fe_i, FeB

Figure 6. PCD carrier lifetimes (Δn @ mpp) on wafers recovered from fully processed solar cells, thus reflecting post-process bulk properties. The carrier lifetime study was part of a Cz-Ga pilot and was meant to assess the potential impact of crystal growth- and cell process-related contamination sources (2016). Metallization and dielectric layers were chemically removed to recover the bulk wafer and determine the post-process carrier lifetime at mpp injection levels. Wafers were both-side passivated (ALD-AlO_x/PECVD-SiN_z) and fired:
(a) Lifetimes post-firing.
(b) Lifetimes post-LID (0.1 Sun @ 30°C for 72h).
(c) Lifetimes post-regeneration (1.0 Sun @ 185°C for 15 min.).

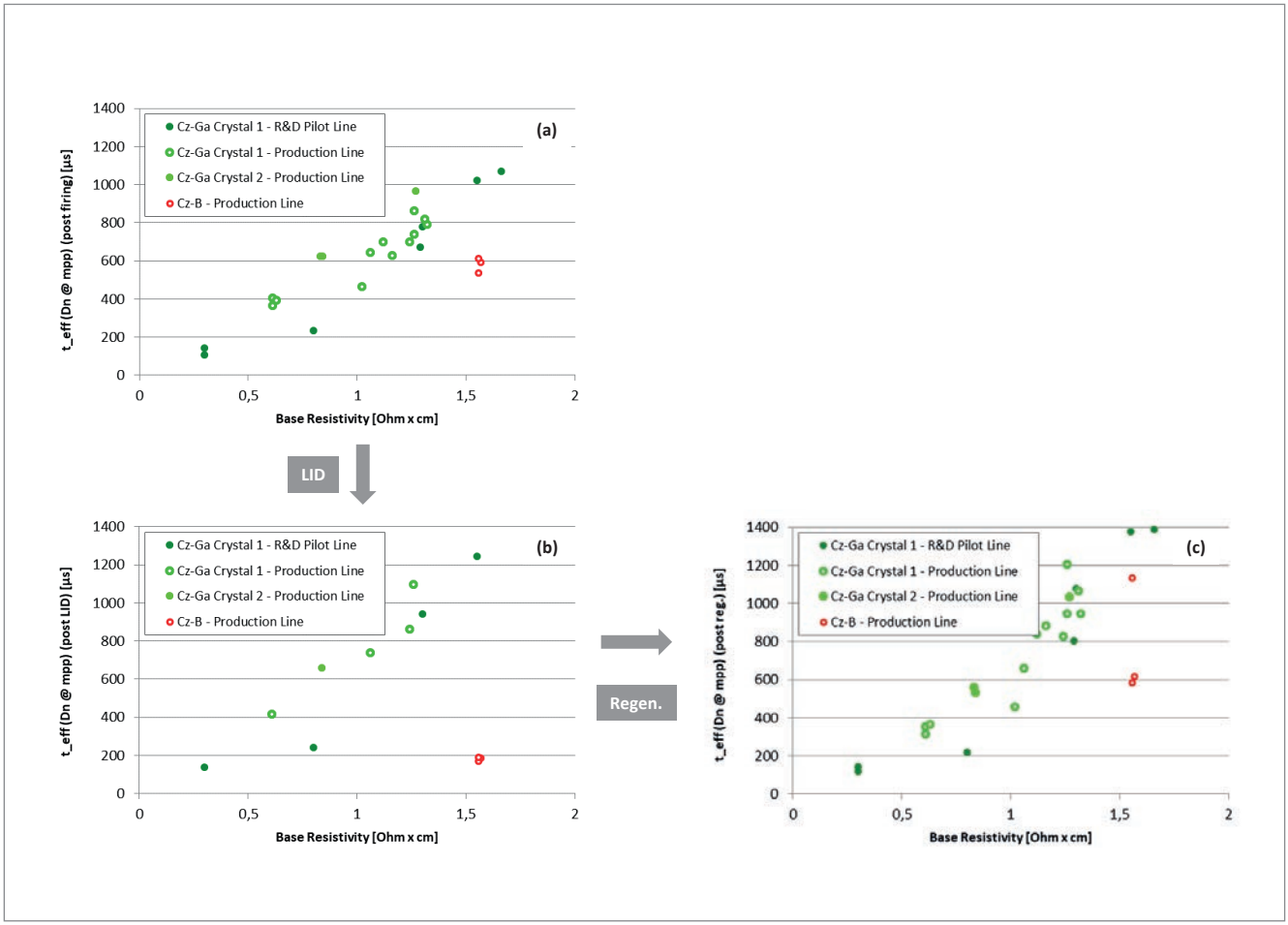

and FeGa as given in Schmidt & Macdonald [40] are employed. It is stressed here that, despite careful sample conditioning, the degree of iron-acceptor association/dissociation is difficult to determine experimentally, with unwanted dissociation/association occurring during sample handling. The results of the SRH analysis were thus parameterized with respect to the degree of dissociation, assuming that the two defects Fe_i and FeX are coexisting (100% corresponds to full dissociation) [42]. Given that dissociation timescales are fairly short (within minutes), and association timescales comparably long (minutes to hours), it can be assumed that samples are dominated by the dissociated Fe_i defect if handled under ambient conditions.

Postulating Fe_i to be the lifetime-limiting defect in Cz-Ga, the iron level, as a free parameter, was adjusted to $[Fe_i] = 1.5\times10^{10}$at/cm³. At this iron level, consistency can be established for the Cz-Ga samples with respect to:

- The experimentally determined carrier lifetimes shown in Fig. 6, assuming the Fe_i defect, i.e. the dissociated state, to be dominating in those measurements.
- The experimentally determined total saturation currents J_{01} in Fig. 4 after subtracting $j_{oe,\,tot}$ ~ 50fA/cm² and $j_{orear,\,tot}$ ~20fA/cm² (refer to the loss analysis in Müller et al. [18]) from J_{01} in order to obtain an estimated $j_{o,mat}$. Note, in particular, that the simulated decrease in material saturation current $j_{o,mat}$ with increasing base resistivity from tail to top follows the measured J_{01} dependence on base resistivity in Fig. 4, again assuming the Fe_i defect to be dominating.

With the Cz-B PERC reference batches having been processed under exactly the same conditions, the same iron level of $[Fe_i] = 1.5\times10^{10}$at/cm³, as an adjustable parameter, was applied in the SRH analysis for B-doped silicon. Comparing the SRH analysis with the experimentally obtained lifetime data (Fig. 6) and *I–V* data (Fig. 4) for the Cz-B samples, an additional background defect must be assumed to be present in the Cz-B

Figure 7. Analytical results for the SRH lifetime and material saturation current at mpp injection levels. The SRH parameters for Fe_i, FeB and FeGa as given in Schmidt & Macdonald [40], and an iron contamination level of $[Fe_i] = 1.5\times10^{10}$at/cm³, are used. With the degree of iron-acceptor dissociation being hard to determine experimentally, the results are parameterized with respect to the degree of dissociation.

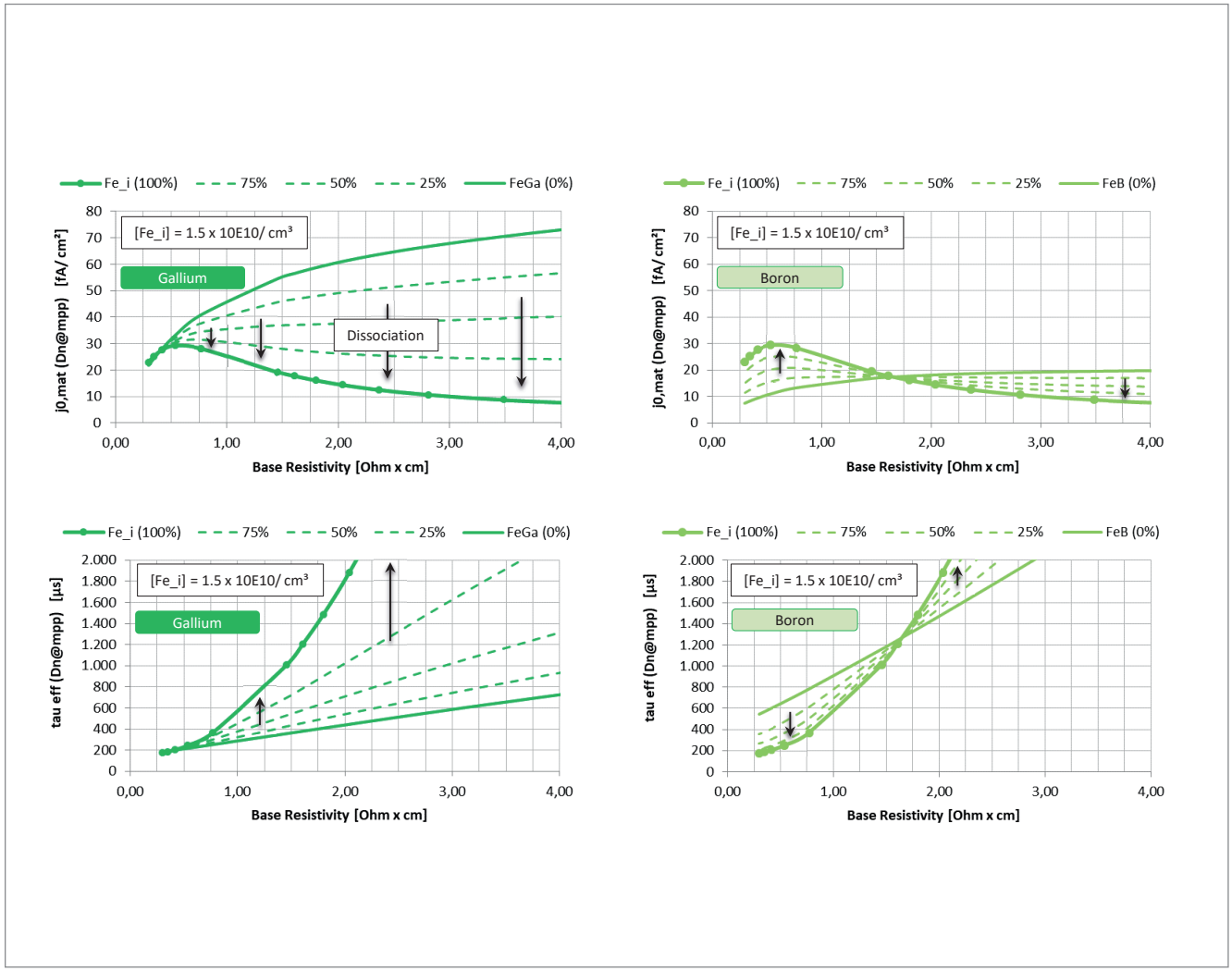

samples, which is limiting the bulk lifetime in Cz-B to lower than Fe_i-limited values, even after regeneration.

Cz-Ga vs. Cz-B – Part 5: FeGa vs. FeB defects – *I–V* data before/after light soaking

Further *qualitative* consistency can be obtained when looking at the relative change in the *I–V* parameters before and after light soaking, despite the fact that the initial and final degrees of FeX dissociation are not known precisely. In this experiment, the regenerated sample set, as shown in Fig. 6, i.e. after 180h exposure to illumination at elevated temperatures, was stored in the dark for 24h and then exposed to the first *I–V* measurement. FeX pairs within the samples were then (partially) dissociated during light soaking at 1 Sun for 10 sec. before the second *I–V* measurement. Fig. 8 shows the resulting observed relative change in $\%_{rel.}$ for selected *I–V* parameters (note that the original units of the *I–V* parameters are indicated in the axis labels, although the relative change is shown). Even though the relative changes are small and well within $1\%_{rel}$, the 'controls' show that the observed effects are real. The differences between the Cz-B and Cz-Ga PERC samples upon (partial) dissociation of the associated initial state before light soaking can, in principle, be explained by the fact that the FeGa defect presents a much stronger recombination centre than the FeB defect [40]. Consequently, the crossover point in Ga-doped silicon (Δn_{CO} (Ga) ~ $0.25\times10^{14}/cm^3$) occurs at a lower injection level than in B-doped silicon (Δn_{CO} (B) ~ $1.4\times10^{14}/cm^3$).

As a result, a higher V_{oc} increase/J_{01} decrease is observed upon (partial) dissociation in Cz-Ga than in Cz-B. The V_{oc} effect is dominating in Cz-Ga-doped silicon. Light soaking for as short as 10 sec. already leads to an overall cell efficiency increase, whereas a slight decrease in cell efficiency is observed for Cz-B-doped silicon, in line with previous studies [41]. Again, a qualitative agreement is obtained for the J_{01} behaviour of the Cz-Ga samples, showing a relative (absolute) decrease of 5% (~5fA/cm²) to 10% (~10fA/cm²) with increasing resistivity from tail (Sec 1) to top (Sec 4). This trend is consistent with the SRH analysis for Cz-Ga in Fig. 7, which shows an increase in the reduction in material saturation current $j_{o,mat}$ with increasing base resistivity upon (partial) dissociation.

In summary, it is inferred from experimental *I–V* data (before and after light soaking), as well as from lifetime data, that bulk recombination in Cz-Ga-doped PERC cells under normal operating conditions (i.e. exposure to light) is strongly influenced by interstitial iron in its dissociated state. In the case of Cz-B, an even more dominating, additional background defect limits the bulk lifetime in Cz-B-doped PERC cells to levels below the Fe_i-limited lifetime – even after regeneration. As a result, the experimental findings suggest superior bulk properties in Cz-Ga over Cz-B in a regenerated state, assuming sufficient Fe-gettering efficiency and sufficiently low Fe_i contamination arising from industrial solar cell production lines.

Given the oversimplified interpretation of the observed results, postulating Fe_i to be the lifetime-limiting SRH defect in our Cz-Ga PERC solar cells, it is suggested that future experimental studies follow (for *practically relevant* experimental investigations of carrier lifetime-limiting defects in Cz-B/Cz-Ga base materials) the methodology outlined in this section. In other words, the *I–V* parameters as well as correlated bulk carrier lifetimes as measured in a post-cell-process condition including regeneration should be investigated, rather than lifetime samples which have not been exposed to the thermal budget and the contamination load associated with a full cell process sequence. In addition, for an improved interpretation of the experimental *I–V* results and the impact of $j_{o,mat}$, numerical simulations should be applied in order to accurately single out the contribution of $j_{o,mat}$ to V_{oc}/J_{01}.

PERC SiO_xN_y/SiN_z – bifacial: *overall* performance assessment and *joint* optimization of front/rear side

Following the industrialization of PERC solar cells in 2012 and onwards, well ahead of the industry, SolarWorld conceived and industrialized another innovative product technology, namely a PERC-based bifacial solar cell, recognizing PERC to be a potential door opener for a highly cost-effective bifacial solar cell. Technology development and business case assessment of the PERC bifacial variant was initiated by the R&D unit at SolarWorld at the beginning of 2014 [43], and has since been adopted by research institutes and several Tier 1 solar cell manufacturers alike [44,45].

Design modifications

Three simple design modifications of the cell rear side are needed in order to derive a PERC bifacial solar cell from the PERC monofacial variant. First, the rear-side dielectric layer stack is adapted for improved rear-side optics (depending on the stack design of the monofacial reference, this may be an optional measure). Second, the full-area rear Al metallization is replaced by a screen-printed Al grid. Third, the LCO pattern is adjusted for optimum overall bifacial performance, since the LCO/Al-finger pitch defines rear-side shading, and the LCO dimensions affect Al-BSF formation at the contact.

As a potential fourth design change, texturing of the rear side can be applied; this is prohibitive for SiO_xN_y/SiN_z rear passivation, which requires a polished surface to ensure good passivation. Similarly, for AlO_x/SiN_z rear passivation deposited

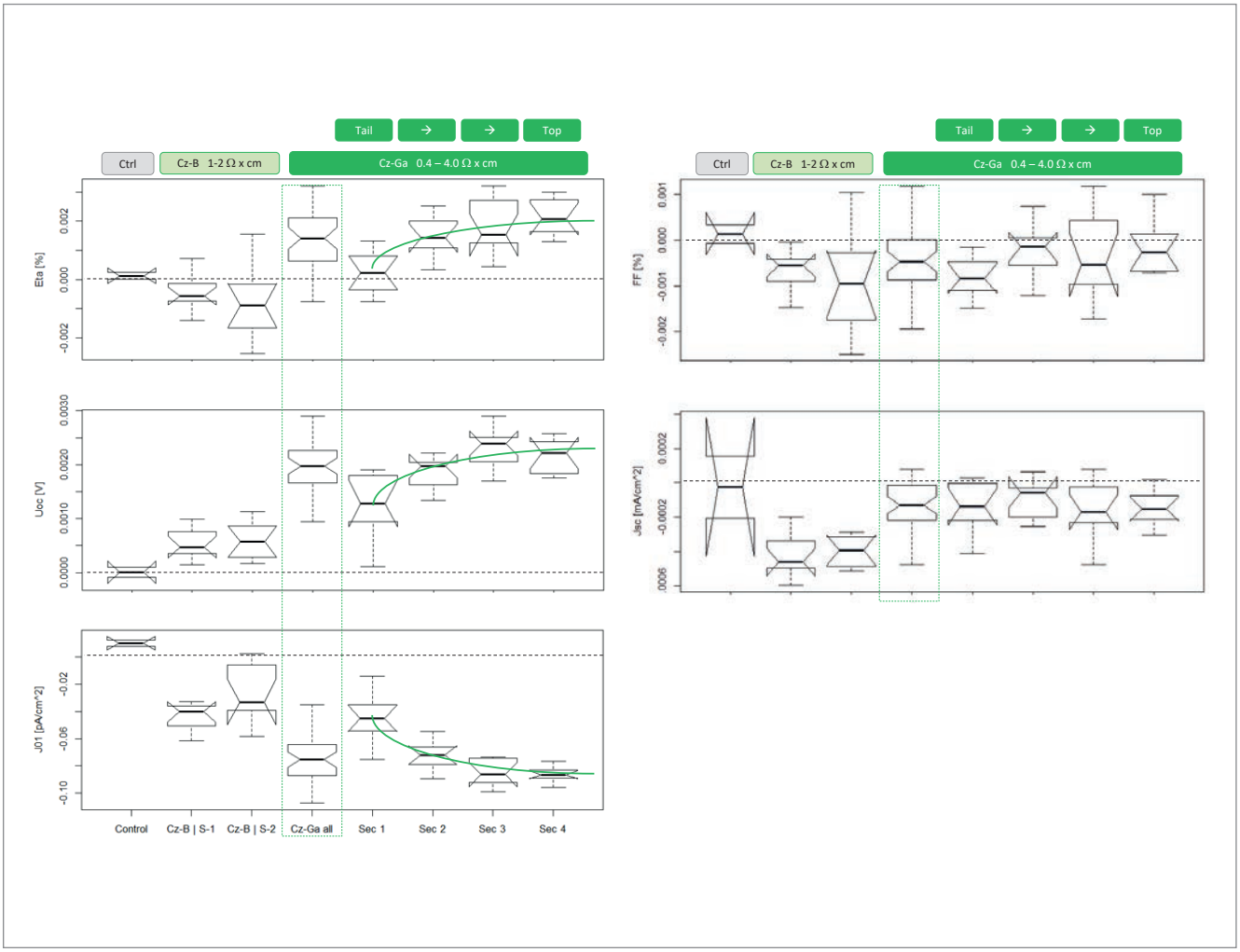

Figure 8. Relative changes in selected *I–V* parameters after light soaking under 1 Sun for 10 sec., leading to *partial* dissociation of Fe-acceptor pairs (note that the original units of the *I–V* parameters are indicated in the axis labels, although the relative change $\%_{rel.}$ is shown). Controls are used to ensure that the small observed effects are real.

by remote PECVD, experimental investigations (carried out on SolarWorld's PERC AlO_x production line in collaboration with Fraunhofer ISE, comparing polished and textured rear surfaces) have shown that a textured rear side significantly decreases the front-side efficiency of a PERC AlO_x/SiN_z bifacial solar cell because of increased light escape from the rear ($J_{sc}\downarrow$) and deteriorating rear passivation ($V_{oc}\downarrow$). As a result, texturing of the rear side for PERC bifacial cells is only suited to high-albedo applications [46].

Metrology

While the above-mentioned design changes are fairly straightforward to implement without additional equipment, the assessment and comparability of bifacial cell *I–V* performance remains up until now non-trivial: measurement techniques and normative rules are still under development [47], and individually chosen *I–V* measurement hardware hinders apple-to-apple comparisons. Particularly misleading – yet still unfortunately in use – are *I–V* measurements using a reflective brass chuck [44]. The use of a reflective chuck leads to an increased short-circuit current (as compared to the use of an absorbent black chuck) and increased fill factors (as compared to the use of contacting bars), since the ohmic resistance of the Al grid (GridRes) is essentially nulled. The main loss channels of a bifacial cell design – transmission losses as well as additional ohmic losses – are (over-)compensated in such a cell *I–V* measurement, which is thus not suitable for bifacial cell design optimization.

Furthermore, in an effort to publish record front- or rear-side efficiencies, bifacial cell designs which are optimized for either front- or rear-side performance and only front- or rear-side efficiency – but not both simultaneously – are reported [44]. Yet, a practically relevant bifacial solar cell design requires joint optimization of front- and rear-side cell efficiencies, which is ideally developed on the basis of an *I–V* measurement setup that:

1. simultaneously applies front-side (1.0kW/m²) and adjustable rear-side (0.XkW/m²) illumination in a double-side measurement, mimicking defined carrier injection levels under bifacial cell operating conditions [46,48];

2. employs a contacting scheme that mimics the resistive cell losses as imposed by a given cell interconnection technology (e.g. five contacting bars for tabbing and stringing of 5BB cells).

Single front-side *I–V* measurements with a black/absorbing background for simplified inline applications are suggested within the 'G_E method', which employs a front-side irradiance of G_E = 1,000W/m² + $\phi_{Jsc} \times G_R$. Here, G_R is typically chosen within 0 to 200W/m² and ϕ_{Jsc} denotes the bifaciality coefficient for the short-circuit current $\phi_{Jsc} = J_{sc}^{rear} / J_{sc}^{front}$. Deviations of the G_E method from a more extensive and accurate two-side measurement are mainly due to cell-to-cell bifaciality variations (since a fixed ϕ_{Jsc} is assumed). The impact of potential nonlinearity of the cell's irradiance/injection dependence has also been considered [49]. It is recommended that two-side measurements are applied in order to validate and thus qualify the G_E method for a given cell type and manufacturing process.

Bifacial cell design rules

As bifacial cell, module and system applications become more sophisticated, future design rules will be developed at the cell, module [45] and system levels as a function of the expected albedo of the particular PV system under consideration. At the cell level, reflection of the rear-side stack and metal shading are clearly the relevant design parameters for rear-side performance tuning; these parameters can be adjusted via rear stack layer thicknesses, LCO pitch and Al-finger width. Optimizing rear-side efficiency is, in general, contrary to front-side optimization, and so a design compromise needs to be made, ideally depending on the expected albedo.

On the basis of the final mono- and bifacial PERC SiO_xN_y/SiN_z design chosen in the R&D baseline process at SolarWorld (design/process BKM 05/2018), the limitations of 5BB p-type PERC bifacial solar cells are addressed with regard to 1) inevitable front-side efficiency losses compared with 5BB p-type PERC monofacial, and 2) rear-side efficiency, and thus bifaciality limitations, as imposed by the optical properties of the rear side.

Front-side efficiency losses: 5BB PERC SiO_xN_y/SiN_z bifacial vs. 5BB PERC SiO_xN_y/SiN_z monofacial

In order to separate the impact of the above-mentioned design modifications on front-side efficiency losses, an experimental run was carried out including three cell types: 1) PERC monofacial reference; 2) PERC bifacial-1, exhibiting the same rear-side stack as the PERC monofacial reference; and 3) PERC bifacial-2, exhibiting a rear-side SiO_xN_y/SiN_z stack optimized for bifacial performance for which the SiN_z capping was

> "A practically relevant bifacial solar cell design requires joint optimization of front- and rear-side cell efficiencies."

significantly reduced. Compared with the monofacial reference, a different, more viscous, Al paste was applied for printing the Al grid on both PERC bifacial-1 and PERC bifacial-2. All other single processes not mentioned are the same for all three cell batches; in particular, the same dashed LCO layout was used for all three cell types.

Fig. 9 depicts the resulting pareto analysis of front-side efficiency losses for the 5BB PERC bifacial solar cells with respect to the 5BB PERC monofacial reference solar cell. *I–V* measurements are carried out using contacting bars (pins) on the front and rear sides. The rear side is fully absorbent (black cloth). CalLab certified reference cells are used for separate calibration of the *I–V* measurements on monofacial and bifacial solar cells. *FF* losses are split into purely resistive losses (FF_R_s) and pure *pFF* losses; the sum of both corresponds to the overall *FF* loss.

As can be seen in Fig. 9, an overall relative loss of 1.5%$_{rel.}$ front-side efficiency already occurs with the printing of an Al grid instead of a full-area Al rear. The relative FF_R_s loss is in good correspondence with the increase in the rear (grid) resistance in the *I–V* measurement. An analytical estimate of the Al rear (grid) resistance based on measured Al finger cross sections is well in line with the observed FF_R_s loss.

Losses are also present for $V_{oc} / J_{sc} / pFF$, which increase with decreasing thickness of the SiN_z capping. The comparison of PERC bifacial-1 and PERC bifacial-2 reveals a reduction in rear-passivation quality and in increased light escape as the SiN_z-capping thickness is reduced. The *pFF* losses are not understood in detail, although it is assumed that inferior local Al-BSF formation when printing an Al grid instead of a full-area Al rear is the driving source. Contrary to the findings in Kranz et al. [50], an inferior quality of the Al-BSF formed in the case of an Al grid print is conjectured from the *I–V* data in the SolarWorld experiments. This is supported by PL V_{oc} images, which show higher recombination activity of the local Al-BSF when compared with a full-area Al metallization. Note that, in contrast to Kranz et al. [50], a different rear-side dielectric (SiO_xN_y/SiN_z) and LCO (dash) design was applied in SolarWorld's implementation. The intricate interplay between rear-side dielectric, LCO-process and LCO-feature size, Al paste and Al laydown, as well as firing conditions, critically affects the Al-Si alloying process and thus the quality of the formed local Al-BSF. This topic will remain crucial to further development of local Al-BSF formation in the PERC bifacial concept based on LCO and Al grid screen printing.

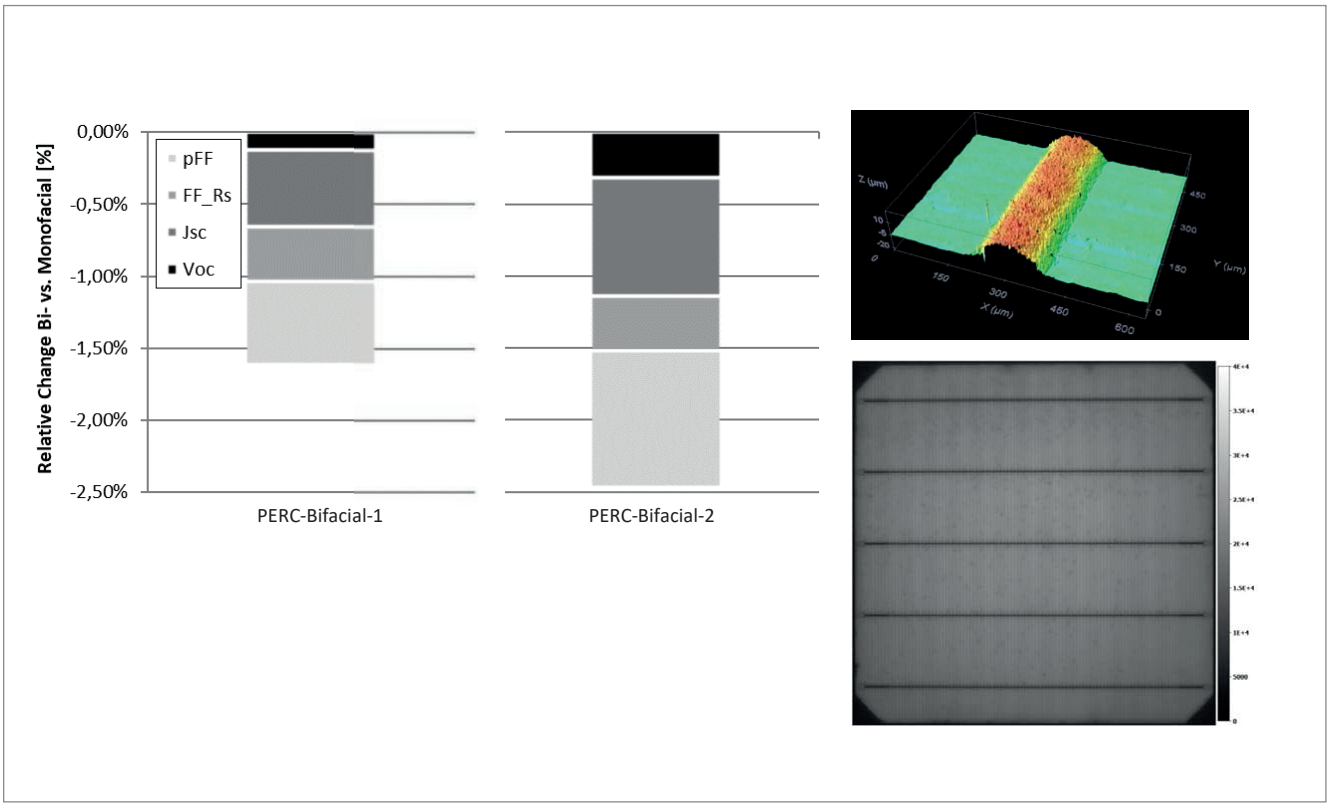

Figure 9. Pareto analysis of front-side efficiency losses for 5BB PERC bifacial solar cells with respect to 5BB PERC monofacial solar cells (BKM 05/2018)]. *I–V* measurements are carried out using contacting bars (pins) on the front and rear sides. The rear side is fully absorbent (black cloth). CalLab-certified reference cells are used for separate calibration of the *I–V* measurements on monofacial and bifacial solar cells.

- **Rear Stack – 1 applied for PERC Bifacial-1 is identical to the rear-side stack of the PERC monofacial reference.**
- **Rear Stack – 2 applied for PERC Bifacial-2 is an adapted rear-side stack optimized for bifacial performance.**
- **LCO-Layouts are identical to the PERC monofacial reference.**

The insets show a 3D scan of an Al finger using a confocal microscope and a PL V_{oc} image of a bifacial solar cell exhibiting black dots (increased non-radiative recombination) in the LCO regions. Note that this feature is not observed for PERC monofacial reference cells.

Rear-side efficiency/bifaciality limitations of PERC SiO_xN_y/SiN_z bifacial solar cells

'Classical' implementations of bifacial solar cells – for example, n-type heterojunction (HJT) pioneered by Sanyo, or n/p-type passivated emitter and rear totally diffused (PERT) cells first brought into mass production by Yingli [45] – feature a full-area BSF (for a front-junction cell) or emitter (for a rear-junction cell) on the rear side; in both cases, this allows passivation functionality to be decoupled from optical functionality (anti-reflection) for the rear-side dielectric to a larger extent. Furthermore, a pyramidal texture can be applied to the rear side in these cell concepts, which allows a high bifaciality in excess of 90%.

In the case of the p-type PERC bifacial cell concept, the rear dielectric needs to simultaneously fulfil passivation and optical requirements. Consequently, a design compromise needs to be made. First and foremost, since texturing of the rear side significantly deteriorates rear-side passivation and internal light reflection in p-type PERC bifacial solar cells, *planar rear* sides are typically in use. Furthermore, since passivation quality deteriorates with decreasing thickness of the SiN_z capping, the optical thickness of the rear stack is not fully optimized for rear light absorption. Consequently, light-capturing from the rear is inherently limited in PERC bifacial.

Another limitation of p-type PERC bifacial is imposed by the use of Al pastes for screen printing instead of Ag pastes, as in the above-mentioned bifacial cell concepts. Given the inferior fine-line printing capability and the increased resistivity of screen-printed Al fingers (finger width ~100µm; resistivity ~20µΩcm) when compared with state-of-the-art Ag paste screen printing (finger width ~30µm; resistivity ~3µΩcm), the rear Al metallization fraction, and thus metal shading, in p-type PERC bifacial is comparably high.

Fig. 10 shows the bifaciality limits as imposed by 1) the reflection-limited external quantum efficiency (EQE) of the planar rear side (stack analogous to PERC bifacial-2), and 2) the Al metallization. Note that the reflection spectrum of a typical AlO_x/SiN_z stack (10nm/100nm) on a planar rear side exhibits a very similar profile to that of the SiO_xN_y/SiN_z stack shown.

A 5BB Al layout with a ~1.0/1.3mm pitch (corresponding to 156/120 Al fingers) and roughly 8.5% Al coverage from the busbars gives rise to a bifaciality of 65%/70% at 200µm as-printed finger width. The high Al coverage/width associated with the busbars was necessary in order to

account for the very low tab-positioning accuracy on the cell rear side of the stringers available at SolarWorld's module manufacturing. Clearly, measurements of the efficiency for bifacial cells using a reflective brass chuck eliminate the resistive losses of the rear Al grid, and finer Al fingers can, in principle, be printed to showcase increased bifaciality using such a measurement configuration without significant *FF* losses in the measurement.

Of practical relevance is the switch to multiwire technology, as it allows the elimination of the rear busbars [45] and thinner Al fingers without sacrificing *FF* as in the 5BB case; this leads to bifacialities exceeding 80% as shown in Fig. 10. As outlined in Dullweber et al. [44] and Nussbaumer et al. [45], the switch to half cells is even more advantageous for bifacial solar cells than for monofacial ones, given the higher operating cell currents, and consequently the increased ohmic losses, for bifacial solar cells. It is therefore clear that PERC bifacial will promote the use of multiwire interconnection and half-cell technology. Even though bifaciality will remain comparably low at 80–85%, the authors believe that PERC bifacial will continue to outperform as a low-cost bifacial solution for typical albedo values in the mid-term.

Summary and outlook

It took more than 20 years to transfer the PERC cell concept from lab to fab [51]. The PERC cell has only been able to enter mass production thanks to 1) equipment suppliers providing the necessary key technologies for *industrially viable* process implementation (most importantly PECVD for rear-side passivation [7,8]), and 2) material suppliers developing Al screen-printing pastes designed for effective local Al-BSF formation. Only as a result of these developments has a simple and cost-effective implementation of PERC solar cells been possible. As an integrated PV module manufacturer, SolarWorld anticipated and significantly contributed to three technology trends which have been guiding the industrial solar cell roadmap since 2012:

- Introduction and process integration of PERC technology in mass production.

Figure 10. Bifaciality limiting factors. Reflection and external quantum efficiency (EQE) spectra for a planar rear side and a SiO_xN_y/SiN_z stack optimized for bifacial performance. For reference, the corresponding spectra are also shown for the front-side ARC on a pyramidal texture (SiO_2/SiN_z). Compared with the monofacial SiO_xN_y/SiN_z stack, the SiN_z capping for the bifacial cell is significantly thinner to allow improved light capture. Short-circuit currents for the front and rear sides are calculated from the EQE spectra to obtain a 'metallization free' bifaciality with an optical limit of $\phi_{Jsc\_optical}$ ~86–88%. Adding metallization on the front (f_met ~4.0%) and rear (f_met 5BB ~8.5%) allows the calculation of cell bifaciality as a function of as-printed Al finger width for 5BB and 0BB configurations. Note that 'effective' metal finger widths need to be applied after cell encapsulation, accounting for light-trapping effects in the module.

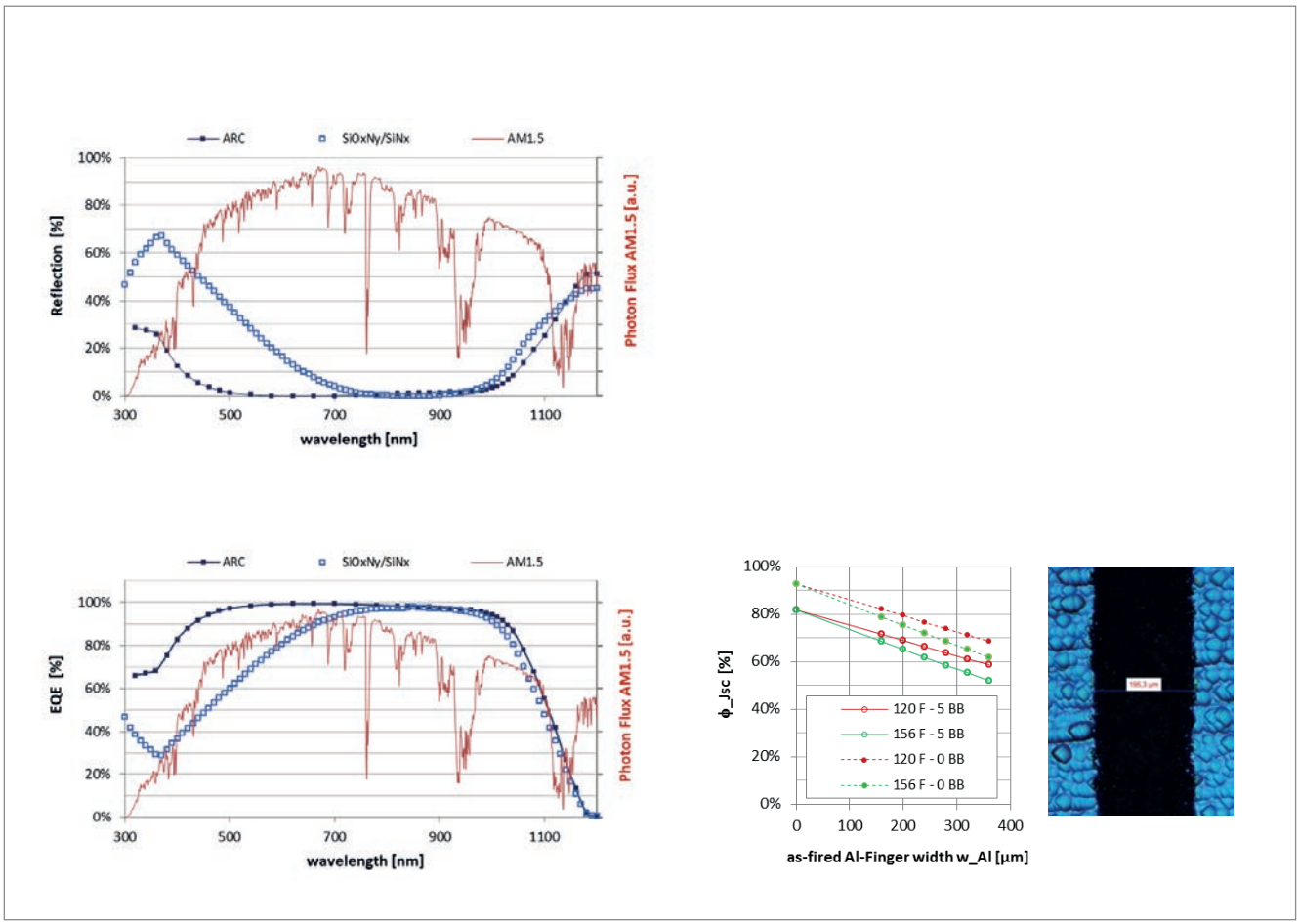

- Introduction of a highly cost-effective PERC-based bifacial solar cell in mass production.
- Conversion from multi- towards monocrystalline wafers, to fully leverage the efficiency potential of PERC [52].

With regard to further increasing the efficiency of p-type PERC solar cells and modules in the short term, the authors foresee the following.

Crystal: gallium – the preferred dopant

On the basis of SolarWorld's investigations of Cz-Ga wafers, further material benchmarks are recommended by comparing CCz-Ga/RCz-Ga and CCz-B/RCz-B technologies with respect to lifetime-limiting defects in *regenerated* solar cells. Monocrystalline Ga, e.g. ideally based on CCz technology, is considered to be a leap in technology that will finally enter mass production.

Cell: selective emitter – certainly, but which technical implementation?

The necessity for introducing selective emitter technology is the general consensus in the context of the 24% PERC roadmap [53]. The more pressing question relates to the preferred technical implementation of SE, and the respective trade-off between efficiency potential and process complexity. Selective etch-back exhibits an inherent advantage over laser doping from PSG with regard to reduced emitter saturation currents in the n^+ region (given the efficient removal of inactive phosphorus), as well as the n^{++} regions (given the avoidance of potential laser damage) [54]. Nevertheless, the process complexity of selective etch-back is higher. The authors consider the choice of SE implementation to be still an open topic and expect technology selection to take place.

Cell: emitter passivation – SiO_2/SiN_x

Thermal oxidation for n^+-type emitters will become widespread.

Cell: rear passivation – cannot beat CVD

With rear passivation representing the smallest loss channel in current 22.0%-efficient p-type Cz PERC solar cells, there is little motivation at the moment to abandon well-established PECVD-based AlO_x/SiN_z deposition and to shift towards, for example, atomic layer deposition (ALD) for Al_2O_3 deposition. On the contrary, CVD offers the flexibility 1) to be used in n-type solar cells using adapted AlO_x/SiN_z stacks for the passivation of p^+-type emitters, or 2) to deposit doped a-Si (PECVD) or poly-Si (LPCVD) layers for the implementation of passivating contacts. The potential option to derive classical n-type PERx cells or p/n-type PERT-like cells employing passivating contacts with the use of existing equipment from current p-type PERC solar cell lines makes PECVD the preferred and compelling process choice for the time being.

Cell: Metallization – active alignment will become standard

With 1) SE becoming the standard and 2) PERC bifacial shares predicted to increase, screen printers with in situ recognition of contact features (e.g. highly-doped regions or local contact openings) and active alignment capability will become standard.

Module: PERC bifacial = accelerating catalyst for multiwire and half-cell module technology

Multiwire technology alleviates the problem of increased ohmic losses in PERC bifacial cells which result from increased Al grid resistance; multiwire therefore enables decreased *FF* losses at increased bifaciality. Half-cell technology, on the other hand, helps to reduce ohmic losses occurring within the interconnecting tabs/wires, and will be even more beneficial for bifacial modules, given their generally higher operating currents. As a result, PERC bifacial will act as a catalyst and push for an accelerated near-term adoption of multiwire, half-cell technology as well as glass-glass encapsulation, i.e. module technologies which SolarWorld has been pursuing since 2013 [22,55]. In addition, the multiwire approach will enable significant further reductions in front finger width and Ag paste consumption.

Before upcoming solar cell technology cycles in crystalline silicon PV (e.g. based on passivating contacts, including HJT as an industrially proven variant) and tandem solar cells later on are in full swing, PERC still holds incremental improvements up its sleeve in crystal, cell and module production technologies which will allow cell efficiencies *in mass production* to be pushed towards 24% [53].

"PERC still holds incremental improvements up its sleeve in crystal, cell and module technologies which will allow cell efficiencies *in mass production* to be pushed towards 24%."

Acknowledgements

The authors would like to give credit to the former SolarWorld staff from R&D, engineering, production, quality assurance, procurement and management responsible for the pioneering work on industrializing PERC technology at SolarWorld, as well as the universities, R&D institutes, key equipment and material manufacturers for their support on this path. We would like to acknowledge our former colleagues in R&D and production transfer: G. Erfurt, E. Schneiderlöchner, A. Münzer, K.-H. Stegemann, M. Wagner, P. Müller, L. Sylla, U. Kirpal, B. Bitnar, R.

Schiepe, P. Richter, S. Gatz, H. Sträter, G. Citarella, C. Merkwitz, A. Fülle, M. Kutzer, M. Georgi, N. Stoddard, E. Good, G. Grupp-Müller, S. Yamanaka, D. Palko, S. Pecis, M. Dulani, A. Rolle, C. Bellmann, U. Mareck, D. Stichtenoth, M. Kipping, T. Roth, A. Froitzheim, K. Kubitz, H. Reetz, L. Oberbeck and the entire team operating the R&D cell pilot line in Freiberg. We would like to thank and give credit to our former R&D partners at the Fraunhofer Institute for Solar Energy Systems ISE , University of Konstanz, Institute for Solar Energy Research in Hamelin (ISFH) as well as our equipment (Centrotherm, Meyer & Burger Germany, Gebr. Schmid, Rena, InnoLas, Asys) and material (Heraeus, Toyo, GigaSolar, Namics , h.a.l.m., USK and 3D Micromac) suppliers, all having done their part in pushing the limits of industrially viable PERC technology. Last, but not least, we would like to thank the Federal Ministry of Economic Affairs and Energy (BMWi) for the funding of PERC solar cell development within the SONNE (FKZ: 0325277A), HELENE (FKZ: 0325777A) and LAURA (FKZ: 0325716A) research projects.

References

[1] IRENA 2015, "Renewable capacity statistics 2015", International Renewable Energy Agency (IRENA), Abu Dhabi.
[2] IRENA 2018, "Renewable capacity statistics 2018", International Renewable Energy Agency (IRENA), Abu Dhabi.
[3] BNEF 2018, "New Energy Outlook 2018: BNEF experience curve for crystalline-silicon PV module prices".
[4] ITRPV 2018, "International technology roadmap for photovoltaic (ITRPV): 2017 results", 9th edn (Mar.) [http://www.itrpv.net/Reports/Downloads/].
[5] Weber, T. et al. 2013, "High volume pilot production of high efficiency PERC solar cells – Analysis based on device simulation", *Energy Procedia*, Vol. 38, pp. 474–481.
[6] Chunduri, S.K. et al. 2018, "PERC solar cell technology 2018 edition, PERC+: How to improve high efficiency crystalline solar cells", TaiyangNews.
[7] Sperlich, H.-P. et al. 2010, "High productive solar cell passivation on Roth&Rau MAiA ® MW-PECVD inline machine – A comparison of Al_2O_3, SiO_2 and SiN_x-H process conditions and performance", *Proc. 25th EU PVSEC*, Valencia, Spain.
[8] Münzer, K.A. et al. 2012, "Technical performance and industrial implementation in favour of centaurus technology", *Energy Procedia*, Vol. 27, pp. 631–637.
[9] Preu, R. et al. 2000, "Laser ablation – A new low-cost approach for passivated rear contact formation in crystalline silicon solar cell technology", *Proc. 16th EU PVSEC*, Glasgow, Scotland.
[10] Agostinelli, G. et al. 2005, "Local contact structures for industrial PERC-type solar cells", *Proc. 20th EU PVSEC*, Barcelona, Spain.
[11] Agostinelli, G. et al. 2005, "Screen printed large area crystalline silicon solar cells on thin substrates", *Proc. 20th EU PVSEC*, Barcelona, Spain.
[12] Schneiderlöchner, E. et al. 2002, "Laser-fired rear contacts for crystalline silicon solar cells", *Prog. Photovolt: Res. Appl.*, Vol. 10, pp. 29–34.
[13] Boschke, T. et al. 2011, "Fully screen-printed PERC cells with laser-fired contacts – An industrial cell concept with 19,5% efficiency", *Proc. 37th IEEE PVSC,* Seattle, Washington, USA, pp. 3663–3666.
[14] Dastgheib-Shirazi, A. et al. 2013, "Relationships between diffusion parameters and phosphorus precipitation during the $POCl_3$ diffusion process, *Energy Procedia*, Vol. 38, pp. 254–262.
[15] Fischer, G. et al. 2015, "Model based continuous improvement of industrial p-type PERC technology beyond 21% efficiency", *Energy Procedia*, Vol. 77, pp. 515–519.
[16] Röder, T.C. et al. 2010, "Add-on laser tailored selective emitter solar cells", *Prog. Photovolt: Res. Appl.*, Vol. 18, pp. 505–510.
[17] Yamanaka, S. et al. 2012, "Optical transparency and surface recombination considerations for high sheet resistance emitter passivation on silicon solar cells", *Proc. 38th IEEE PVSC*, Austin, Texas, USA, pp. 001166–001171.
[18] Müller, M. et al. 2017, "Loss analysis of 22% efficient industrial PERC solar cells", *Energy Procedia*, Vol. 124, pp. 131–137.
[19] HELENE research project, under Contract No. 0325777.
[20] Zhou, T. et al. 2016, "Different dielectrics deposited by PECVD for the industrial manufacturing of PERC solar cells", *Proc. 31st EU PVSEC*, Hamburg, Germany.
[21] Richter, P.L. et al. 2015, "Progress in fine-line metallization by co-extrusion printing on cast monosilicon PERC solar cells", *Sol. Energy Mater. Sol. Cells,* Vol. 142, pp. 18–23.
[22] Schaarschmidt, M. et al. 2011, "Method for contacting and connecting solar cells and solar cell combination produced by means of said method", Patent WO/2011/147388.
[23] Müller, M. 2016, "Reporting effective lifetimes at solar cell relevant injection densities", *Energy Procedia*, Vol. 92, pp. 138–144.
[24] Wolny, F. et al. 2017, "Study of the bulk lifetime and material saturation current density of different p-type monocrystalline silicon materials", *Energy Procedia*, Vol. 124, pp. 235–239.
[25] Krause, A. et al. 2016, "Plastic deformation as an origin of dislocations in cast mono", *Energy Procedia,* Vol. 92, pp. 833–838.
[26] Stoddard, N. et al. 2018, "NeoGrowth Silicon: A new high purity, low-oxygen crystal growth

technique for photovoltaic substrates", *Prog. Photovoltaics: Res. Appl.*, Vol 26, pp. 324–331.
[27] PV-Tech 2015, "SolarWorld touts 21.7% PERC world record efficiency", News Report, [https://www.pv-tech.org/news/solarworld_touts_21.7_perc_world_record_efficiecny].
[28] PV-Tech 2016, "SolarWorld reaches 22% efficiency in p-type PERC cell", News Report [https://www.pv-tech.org/news/solarworld-reaches-22-efficiency-in-p-type-perc-cell].
[29] Schmidt, J. et al. 1997, "Investigation of carrier lifetime instabilities in Cz-grown silicon", *Proc. 26th IEEE PVSC*, Anaheim, California, USA, pp. 13–18.
[30] Glunz, S.W. et al. 1999, "Comparison of boron-doped and gallium-doped p-type Czochralski silicon for photovoltaic application", *Prog. Photovoltaics: Res. Appl.*, Vol 7, pp. 463–469.
[31] Tadashi, S. et al. 2000, "Overview of light degradation research on crystalline silicon solar cells", *Prog. Photovolt: Res. Appl.,* Vol 8, pp. 537–547.
[32] Lauermann, T. et al. 2010, "Large area solar cells made from degradation-free, low resistivity gallium doped Cz wafers", *Proc. 25th EU PVSEC*, Valencia, Spain.
[33] Fertig, F. et al. 2017, "Mass production of p-type Cz silicon solar cells approaching average stable conversion efficiencies of 22 %", *Energy Procedia*, Vol. 124, pp. 338–345.
[34] Walter, D. et al. 2016, "Realistic efficiency potential of next-generation industrial Czochralski-grown silicon solar cells after deactivation of the boron-oxygen-related defect center", *Prog. Photovolt: Res. Appl.*, Vol 24, pp. 920–928.
[35] Weber, E.R. 1983, "Transition metals in silicon", *Appl. Phys. A*, Vol. 30, No. 1, pp. 1–22 [https://doi.org/10.1007/BF00617708].
[36] Ludwig, G.W. & Woodbury, H.H. 1962, "Electron spin resonance in semiconductors", *Solid State Phys.,* Vol. 13, pp. 223–304.
[37] Istratov, A., Hieslmair, H. & Weber, E. 1999, "Iron and its complexes in silicon", *Appl. Phys. A,* Vol. 69, No. 1, pp. 13– 44 [https://doi.org/10.1007/s003390050968].
[38] Macdonald, D. et al. 2004, "Iron detection in crystalline silicon by carrier lifetime measurements for arbitrary injection and doping", *J. Appl. Phys.,* Vol. 95, 1021.
[39] Macdonald, D. et al 2005, "Formation of iron-acceptor pairs in crystalline silicon", *J. Appl. Phys.*, Vol. 98, 083509.
[40] Schmidt, J. & Macdonald, D. 2005, "Recombination activity of iron-gallium and iron-indium pairs in silicon", *J. Appl. Phys.,* Vol. 97, 113712.
[41] Schmidt, J. 2005, "Effect of dissociation of iron-boron pairs in crystalline silicon on solar cell properties", *Prog. Photovolt: Res. Appl.*, Vol 13, pp. 325–331.
[42] Naerland, T. et al. 2017, "On the recombination centers of iron-gallium pairs in Ga-doped silicon", *J. Appl. Phys.,* Vol. 122, 085703.
[43] Handelsblatt 2014, "Asbeck versucht Neustart: Ex-Sonnenkönig kündigt neue Modultechnik an", Press Release [http://www.genios.de/presse-archiv/artikel/HB/20141215/asbeck-versucht-neustart/6E27CF9D-B436-48EF-9CEA-EFC3080CD8F5.html].
[44] Dullweber, T. et al. 2018, "Industrial implementation of bifacial PERC+ solar cells and modules: Present status and future opportunities", *Photovoltaics International,* 38th edn, pp. 46–55.
[45] Nussbaumer, H. et al. 2018, "State-of-the-art bifacial module technology", *PV Tech Power,* Vol. 16, pp. 60–80.
[46] Wöhrle, N. et al. 2017, "Understanding the rear-side layout of p-doped bifacial PERC solar cells with simulation driven experiments", *Energy Procedia*, Vol. 124, pp. 225–234.
[47] Fakhfouri, V. 2016, "IEC 60904-1-2: Measurement of current-voltage characteristics of bifacial photovoltaic devices", 3rd Bifi PV Workshop, Miyazaki, Japan.
[48] Ramspeck, K. et al. 2017, "Measurement techniques for bifacial solar cells", 4th Bifi PV Workshop, Konstanz, Germany.
[49] Rauer, M. et al. 2017, "Bifacial solar cells under single- and double-sided illumination: Effect of non-linearity in short-circuit current", 4th Bifi PV Workshop, Konstanz, Germany.
[50] Kranz, C. et al. 2016, "Analysis of local aluminum rear contacts of bifacial PERC+ solar cells", *IEEE J. Photovolt.,* Vol. 6, No. 4, pp. 830–836.
[51] Blakers, A.W. 1989, "22.8% efficient silicon solar cell", *Appl. Phys. Lett.,* Vol. 55, No. 13, pp. 1363–1365.
[52] Colville, F. 2018, "China-531 to accelerate demise of multi; polysilicon consumption decline to 3g/W by 2022", PV Tech News Report (Sep).
[53] Min, B. et al. 2017, "A roadmap toward 24% efficient PERC solar cells in industrial mass production", *IEEE J. Photovolt.,* Vol. 7, pp. 1541–1550.
[54] Ye, F. et al. 2016, "22.13% efficient industrial p-type mono PERC solar cell", DOI: 10.1109/PVSC.2016.7750289.
[55] BINE-Projektinfo 10/2013, ISSN 0937-8367, "Development of high-efficiency solar cells and modules" [http://www.bine.info/fileadmin/content/Presse/Projektinfos_2013/PM_10_2013/ProjektInfo_1013_engl_internetx.pdf].

About the Authors

Phedon Palinginis joined SolarWorld in 2006 and has led the solar cell development group since 2015, with a focus on monocrystalline p-type PERC technology. Prior to that, he was in charge of technology assessment and selection over the entire c-Si PV value chain. Phedon holds

a diploma degree in physics from the University of Karlsruhe and has worked as a doctoral and postdoctoral researcher at the University of Oregon and the University of California Berkeley respectively, on nonlinear optical properties of compound semiconductor nanostructures.

Christian Kusterer received his doctorate in 2006 from the University of Bonn, with a thesis in solid state chemistry. He joined SolarWorld in 2007, and since 2011 he has been responsible for the development and improvement of wet chemistry processes for solar cell processing, including the suppression of process-related contamination sources. Christian has been heavily involved in assessing alternative etching technologies, equipment and processes within feasibility, prototyping and technology transfer, as well as production ramp-up projects.

Stefan Steckemetz received his diploma degree in technical physics from the University of Applied Sciences Aachen in 1993. He then worked on crystalline silicon solar cells at ISFH and Sunways AG, before joining SolarWorld in 2006, where he has been focusing on screen-printing metallization for high-efficiency solar cells in production and R&D. In parallel, Stefan has been investigating and assessing dual/double screen printing as well as extrusion and stencil printing as metallization technology alternatives.

René Köhler joined SolarWorld in 2010. Working within the solar cell development group at SolarWorld, he was responsible for the process development of thin-film coatings and high-temperature processes. Before he joined SolarWorld, he worked in the field of amorphous silicon/crystalline silicon heterojunction solar cells. He holds a diploma degree in technical physics from the Technical University of Ilmenau.

René Härtwig joined SolarWorld in 2002. As an industrial specialist in the field of mechatronics, he first worked as shift supervisor at the solar cell manufacturing site in Freiberg from 2003 until 2012, before taking over the lead of solar cell pilot line operations within R&D in 2012. René and his team ensured stable baseline operation and highly reliable execution of experiments on the R&D pilot line.

Torsten Weber received his diploma degree in physics from the University of Hanover in 2006. He then joined SolarWorld as a senior R&D engineer and project manager, and was responsible for the transfer and integration of high-efficiency cell concepts from feasibility studies to high-volume manufacturing. He is now with Heliatek GmbH, where he focuses on process integration and yield enhancement of OPV.

Matthias Müller received his diploma degree in physics from Leipzig University in 2009, followed by his Ph.D. from Leibniz University Hannover in 2014. From 2007 he worked for Q-Cells SE, GP Inspect GmbH, Magdeburg-Stendal University of Applied Sciences and SolarWorld Innovations GmbH, before joining TU Bergakademie Freiberg in 2017 as the PV group leader at the Institute of Applied Physics. His field of research combines numerical device simulation with solar cell reliability and energy yield calculations.

Gerd Fischer received his Ph.D. in chemistry from TU Dresden. Prior to joining SolarWorld, he worked at Infineon and Qimonda. He joined SolarWorld Innovation in 2008 and worked as a project manager for PERC optimization. Gerd has been instrumental in introducing numerical device simulation for multi- and monocrystalline solar cells at SolarWorld. Since 2017 he has been a professor of inorganic chemistry at the University of Applied Sciences Zittau/Goerlitz.

Dirk Holger Neuhaus holds a Ph.D. from the University of New South Wales. He was a development engineer at Pacific Solar Pty Ltd., and worked for more than 15 years at SolarWorld, where he initially was responsible for quality assurance and technology in cell production, and later headed the global R&D activities along the entire value chain. Holger joined Fraunhofer ISE in 2018 and is in charge of module technology.

Enquiries
Phedon Palinginis
Email: phedon_pv@yahoo.com

Dirk Holger Neuhaus
Email: holger.neuhaus@ise.fraunhofer.de